GUSTAVO DE ALMEIDA ANDOLPHO

EXPLORING EPR AND NMR PARAMETERS OF BENZOTHIAZOLE METALLIC COMPLEXES WITH RHENIUM: IMPLICATIONS FOR NEW MRI PROBES

LAVRAS – MG

2022

GUSTAVO DE ALMEIDA ANDOLPHO

EXPLORING EPR AND NMR PARAMETERS OF BENZOTHIAZOLE METALLIC COMPLEXES WITH RHENIUM: IMPLICATIONS FOR NEW MRI PROBES

Dissertação apresentada à Universidade Federal de Lavras, como parte das exigências do Programa do Pós-Graduação em Agroquímica, área de concentração em Química Computacional, para obtenção do título de mestre.

Profa. Dr. Elaine Ferreira Fontes da Cunha

Orientadora

LAVRAS – MG

2022

Ficha catalográfica elaborada pelo Sistema de Geração de Ficha Catalográfica da Biblioteca Universitária da UFLA, com dados informados pelo(a) próprio(a) autor(a).

Andolpho, Gustavo de Almeida.
Exploring EPR and NMR parameters of benzothiazole metallic complexes with Rhenium : Implications for new MRI probes / Gustavo de Almeida Andolpho. - 2022.
74 p. : il.

Orientador(a): Elaine Ferreira Fontes da Cunha.

Dissertação (mestrado acadêmico) - Universidade Federal de Lavras, 2022.
Bibliografia.

1. Cálculos de parâmetros de NMR. 2. Cálculos de parâmetros de EPR. 3. Efeitos relativísticos. I. da Cunha, Elaine Ferreira Fontes. II. Título.

GUSTAVO DE ALMEIDA ANDOLPHO

EXPLORING EPR AND NMR PARAMETERS OF BENZOTHIAZOLE METALLIC COMPLEXES WITH RHENIUM: IMPLICATIONS FOR NEW MRI PROBES

EXPLORANDO PARÊMETROS DE RMN E RPE DE COMPLEXOS METÁLICOS DE BONZOTIAZOL COM RÊNIO: IMPLICAÇÕES PARA NOVAS SONDAS DE IRM

Dissertação apresentada à Universidade Federal de Lavras, como parte das exigências do Programa do Pós-Graduação em Agroquímica, área de concentração em Química Computacional, para obtenção do título de mestre.

APROVADA em 28 de janeiro de 2022

Dr. Daniel Henriques Soares Leal UNIFEI

Dr. Paulo Augusto Netz UFRGS

Profa. Dr. Elaine Ferreira Fontes da Cunha
Orientadora

LAVRAS – MG

2022

Aos meus pais, Edilaine e Pedro,

aos meus avós, Edival, Maria de Lourdes e Marilene,

ao meu irmão, João Pedro,

aos meus tios e primos,

a Camilla, por todo o apoio e companheirismo.

Dedico

ACKNOWLEDGEMENTS

I would like to thank my family, especially my parents, Edilaine and Pedro, my brother, João Pedro, my grandparents, Edival, Maria de Lourdes and Marilene, my aunts and uncles, Edivane, Paulo, Adriana and Fernando, and my cousins, Marina, Luiza, Angela, and Rafael, thank you all for all the love, support, and for always believed and encouraged me.

I would also like to thank my girlfriend, Camilla, who always gives me the strength to keep going, for always believing in me and not letting me give up. Thanks for all the love, companionship, and friendship.

To professor Teodorico, for his guidance, trust, and teachings. Thank you for all the support and opportunities. To professor Elaine for being my advisor.

All my friends from Lavras and Rio Claro, for the moments of relaxation, fun, and all the companionship, even in pandemic times.

To all my colleagues from the Computational Chemistry Laboratory – MOLECC.

The Federal University of Lavras, the Chemistry Department, and the Agrochemistry program for the opportunities.

O presente trabalho foi desenvolvido com o apoio do Conselho Nacional de Desenvolvimento Científico e Tecnológico (CNPq). Also, thanks the CAPES and FAPEMIG for support.

To the other friends and colleagues who, in one way or another, supported me.

Thank you very much!

RESUMO GERAL

O Câncer é uma das principais causas de morte no mundo, entre todos os tipos de câncer, o câncer de mama é um dos mais comuns e tem uma alta taxa de mortalidade. Para evitar os casos de morte, o diagnóstico precoce é essencial para um tratamento bem sucedido. Neste caso, as técnicas de ressonância magnética, que são frequentemente utilizadas para o diagnóstico, precisam de um agente de contraste (AC) para melhorar as imagens obtidas. O complexo ReABT, que é o complexo Re(CO)3(NNO) conjugado com 2-(4'-aminofenil)benzotiazol, é apresentado como candidato para atuar como sonda espectroscópica ao invés dos tradicionais ACs. Em linha com este cenário, este estudo foi divido em duas partes, a primeira foi focalizada nos parâmetros da Ressonância Paramagnética Eletrônica (RPE) que modulam a ação de ressonância magnética deste complexo. Esta parte do estudo foi realizada avaliando a influência do núcleo de Rênio nos átomos de Hidrogênio das moléculas de água em diferentes ambientes químicos (fase gasoso, solução e dentro do sítio ativo da enzima PI3K) no nível teórico, utilizando métodos DFT. Além disso, os efeitos relativísticos nos resultados da RPE foram avaliados usando a implementação ZORA e uma análise termodinâmica foi realizada para confirmar a estabilidade do ReABT. A segunda parte deste trabalho está centrado no estudo dos parâmetros de ressonância magnética nuclear (RMN), constante de blindagem (σ), do complexo ReABT. O melhor protocolo de cálculo foi definido, por um modelo HCA, com o funcional PBE0 e a implementação ZORA no sistema Hamiltoniano e nos conjuntos de bases. Os resultados indicam que o ReABT pode ser usado como sonda espectroscópica, sendo promissor para aplicação no diagnóstico de medicina nuclear do câncer de mama.

Palavras-chave: Câncer de Mama. Efeitos Relativísticos. RMN. RPE. Agente de Contraste

GENERAL ABSTRACT

Cancer is a leading cause of death worldwide, among all cancer types, breast cancer is one of the most common and has a high mortality rate. To avoid death cases, early diagnosis is essential to a successful treatment. In this case, Magnetic Resonance Imaging (MRI) techniques, which are often used for the diagnosis, need a contrast agent (CA) for improving the obtained images. The complex ReABT, which is the complex $Re(CO)_3(NNO)$ conjugated with 2-(4'-aminophenyl)benzothiazole, presented as a candidate for acting as a spectroscopic probe instead of the traditional CAs. In line with that scenario, this study was divided into two parts, the first one was focused on the Electronic Paramagnetic Resonance (EPR) parameters that modulate the MRI action of this complex. This part of the study was carried out by evaluating the influence of the rhenium nucleus on the hydrogen atoms of water molecules in different chemical environments (gas phase, solution, and inside PI3K enzyme active site) at the theoretical level using DFT methods. In addition, relativistic effects on the EPR results were evaluated using ZORA implementation and a thermodynamic analysis was performed to confirm the stability of ReABT. The second part of this work is focused on the study of the NMR parameters, shielding tensors (σ), of the complex ReABT. The best calculation protocol has been defined, by an HCA model, with the PEB0 functional and the ZORA implementation on the hamiltonian system and basis sets. The results indicate that ReABT can be used as spectroscopic probes, being promising for application in the nuclear medicine diagnosis of breast cancer.

Keywords: Breast Cancer. Relativistic Effects. NMR. EPR. Contrast Agent.

LIST OF FIGURES

FIRST PART

SECOND PART

Article 1

Article 2

LIST OF TABLES

SECOND PART

Article 1

Article 2

SUMMARY

FIRST PART

SECOND PART

FIRST PART

1. INTRODUCTION

Breast cancer is one of the diseases with the most positive cases and is responsible for many deaths annually in the world. The main topic to decrease these rates is the early diagnosis. For that, several techniques could be used, such as mammography, ultrasonography, magnetic resonance imaging (MRI), positron emission tomography (PET), computed tomography, and single-photon emission computed tomography (SPECT).

The most used techniques are mammography and ultrasonography. However, in several cases, these techniques are not enough for a correct and precise diagnosis. So, the use of other techniques is needed, such as PET, SPECT, computed tomography, and MRI.

Magnetic resonance imaging is a widely used technique, which is based on NMR parameters to generate an image. Meantime, the images generated by the MRI are often not of high quality, requiring the use of contrast agents (CA's), which alter relaxation parameters to improve the quality of the images and interact with important proteins.

Several studies indicate that the phosphoinositide 3-kinase (PI3K) protein, responsible for several mechanisms of cell proliferation, is responsible for the proliferation of breast cancer cells. So, CAs can be able to bind to these proteins to perform an accurate diagnosis.

Several studies point out that phenylbenzothiazole derivatives show antitumor activity, thus it is crucial the search for spectroscopic probes with a metallic center, which can bind to a phenylbenzothiazole derivative. Among these compounds, we highlight those with Rhenium as a metallic center, bonded to three carbonyls and (N-(2-pyridylmethyl)-aminoacetic acid ($Re(CO)_3(NNO)$ complex) conjugated to 2-(4'-aminophenyl) benzothiazole.

This compound can in principle be able to act as a spectroscopic probe, being able to change the hyperfine coupling constants and the chemical shift values. To evaluate this effect, computational calculations were performed to evaluate several aspects, such as the binding mode between the compound and the PI3K enzyme, as well as to calculate EPR and NMR parameters.

Density Functional Theory (DFT) calculations for optimization of geometry, chemical shifts, hyperfine coupling constants were performed. In addition, molecular docking calculations were carried out to evaluate the potential of this substance as a spectroscopic probe

for MRI. In this perspective, the influence of the enzymatic environment, solvent, and relativistic effects were evaluated by different theoretical approaches.

2. THEORETICAL REFERENCE

2.1. Breast Cancer

Breast cancer, like other cancers, is caused by a disorderly multiplication of breast cells, generating abnormal cells that can form a tumor. According to Instituto Nacional do Câncer – INCA, predictions indicate that over 66,000 new cases of breast cancer will arise in Brazil, which represent approximately 30% of cases of cancer among Brazilian women (INCA, 2019).

Of the total deaths from cancer in 2017 in Brazil, about 16% were due to breast cancer, totaling more than 16 thousand fatalities according to the Ministry of Health (INCA, 2019). This disease can be acquired or hereditary and can be influenced by environmental, emotional, food, and reproductive factors (GALVÃO; MARTINS; IBIAPINA; ANDRADE *et al.*, 2011).

The early discovery of the disease is one of the main factors for the successful treatment of the disease. Thus, the improvement and discovery of more efficient techniques for early identification is an important step towards reducing the number of deaths. The main method for the diagnostic of tumors is through imaging exams, which in addition to identifying tumors, assist in the time of possible surgery, because the images generated are of high quality, allowing better visualization of the region of the intervention (JAFARI; SAADATPOUR; SALMANINEJAD; MOMENI *et al.*, 2018; WAKS; WINER, 2019).

2.1.1. Diagnosis

Several techniques can be applied to diagnose breast cancer, where each technique has its peculiarities. Among them, we can highlight mammography, ultrasonography, magnetic resonance imaging (MRI), Positron emission tomography (PET), computed tomography, and Single-photon emission computed tomography (SPECT). The last three do not apply to routine

exams due to their high cost and incidence of radiation, being recommended for supplementary diagnostic (HE; CHEN; TAN; ELINGARAMI *et al.*, 2020).

The most used techniques are mammography (MG), ultrasonography (US), and MRI (HE; CHEN; TAN; ELINGARAMI *et al.*, 2020). The first one consists of an X-ray scan that can find a mass in the tissues, but it cannot identify whether it is cancer. The MG is important for diagnosis due to its low cost and its good sensitivity and specificity, however many times this technique cannot be applied or is not good enough to correctly identify breast cancer (BARBA; LEÓN-SOSA; LUGO; SUQUILLO *et al.*, 2021; HE; CHEN; TAN; ELINGARAMI *et al.*, 2020; JAFARI; SAADATPOUR; SALMANINEJAD; MOMENI *et al.*, 2018).

To improve diagnosis, ultrasonography could be used. This non-invasive technique finds tumors, but some of the US methods cannot distinguish between benign or malignant tumors due to their low definition and resolution. Small masses or atypical tissues are not also easily identified and are often neglected, once a professional must interpret the exam (BARBA; LEÓN-SOSA; LUGO; SUQUILLO *et al.*, 2021; HE; CHEN; TAN; ELINGARAMI *et al.*, 2020).

Just like the US, Magnetic Resonance Imaging (MRI) is a non-invasive technique. MRI has characteristics that make it a highly sensitive technique, being able to identify tumors at different stages and locations. Its application is recommended for patients of any age or high risk and can also be used to accompany treatment (BARBA; LEÓN-SOSA; LUGO; SUQUILLO *et al.*, 2021; HE; CHEN; TAN; ELINGARAMI *et al.*, 2020).

To help improve the success of the MRI technique, patients use a contrast agent (CA), a substance that improves the sensitivity of imaging on the region in the exam. This CA improves the visualization of the tumor, providing imaging that allows doctors to identify, find and accompany the lesion and the tissues around (BARBA; LEÓN-SOSA; LUGO; SUQUILLO *et al.*, 2021; JAFARI; SAADATPOUR; SALMANINEJAD; MOMENI *et al.*, 2018). The nuances of MRI and its contrast agents will be discussed further in this text. However, we will discuss initially crucial concepts considering NMR and EPR techniques.

2.2. Nuclear Magnetic Resonance

Nuclear Magnetic Resonance (NMR) is an important technique for determining molecular structure and geometry (SKOOG; HOLLER; CROUCH, 2017). The property of interest of this technique is the nuclear spin, for the nucleus to be active in the NMR spectroscopy, the spin must be different from zero. NMR spectra are obtained from the nuclear spin transitions undergone by the nuclei submitted to a magnetic field (B_0), as shown in equations 1 and 2. The energy involved in these transitions is quantized, with the chemical shift being one of the fundamental parameters of the NMR technique, which is directly related to the frequency of radiation absorbed by the nucleus that undergoes this process (PAVIA; LAMPMAN; KRIZ; VYVYAN, 2010).

$$\mu = \gamma I \hbar \qquad (1)$$

where μ is the nuclear magnetic moment, γ is the nucleus gyromagnetic ratio, I is the spin and $\hbar$ is the Planck constant.

$$E = -\mu B_0 \qquad (2)$$

where E is the Energy, μ is the nuclear magnetic moment B_0 is the magnetic field.

In NMR, the sample is subjected to a magnetic field, however, the interaction of the field with the electrons generates an induced magnetic field, these magnetic fields are related by a proportionality constant called the shielding constant. The chemical shift (δ) of the various nuclei present in a molecule depends on the electronic environment of each one, which is described by the shielding constant (σ) (Equation 3) (PAVIA; LAMPMAN; KRIZ; VYVYAN, 2010).

$$\delta = \sigma_{ref} - \sigma_{calc} \qquad (3)$$

To understand the neighborhood of the nucleus, the NMR provides another parameter called coupling constant (J). Among the NMR parameters, two of them, chemical shifts, and coupling constants, can help to elucidate the structural characteristics of the compound (PAVIA; LAMPMAN; KRIZ; VYVYAN, 2010).

These NMR parameters can be applied to medical applications, helping the diagnosis and treatment of several diseases. One of the techniques that used the NMR principles is a magnetic resonance imaging (MRI) technique that will be discussed in further sections (SKOOG; HOLLER; CROUCH, 2017).

2.2.1. Electronic Paramagnetic Resonance

Electronic Paramagnetic Resonance (EPR) is a technique derived from NMR, but EPR only works for compounds with unpaired electrons. This technique used the electronic g tensors and the hyperfine coupling constant (A) (FRECUS; RINKEVICIUS; ÅGREN, 2013).

After removing the radiofrequency that magnetized the molecule, the relaxation process takes place, where the spins will return to equilibrium. Two relaxation processes can occur independently, longitudinal relaxation (T1), or spin-network relaxation, which describes the return to balance in the direction of the magnetic field and transversal relaxation (T2), or spin-spin relaxation, and represents the decay of magnetized energy perpendicular to the magnetic field (CARNEIRO; VILELA; DE ARAUJO; BAFFA, 2006).

Spin relaxation is measurable, from the time taken to return to equilibrium, for T1 (Equation 4), and the time taken for the loss of magnetization, in T2 (Equation 5), and is used for applications in images (GONÇALVES; PEIXOTO; DA CUNHA; RAMALHO, 2014).

$$R_1 = \frac{1}{T_1} \cong \frac{1}{15}\frac{S(S+1)g_e^2\beta^2 g_N^2\beta_N^2}{\hbar^2 r^6} + \left(\frac{A}{\hbar}\right)^2 \frac{S(S+1)}{3}\left[\frac{2\tau_e}{1+(\omega_I\tau_e)^2}\right] \qquad (4)$$

$$R_2 = \frac{1}{T_2} \cong \frac{1}{15}\frac{S(S+1)g_e^2\beta^2 g_N^2\beta_N^2}{\hbar^2 r^6} + \left(\frac{A}{\hbar}\right)^2 \frac{S(S+1)}{3}\left[\tau_C + \frac{\tau_c}{1+(\omega_s\tau_e)^2}\right] \qquad (5)$$

In these two equations, we can see the dependence of the relaxations time constant (T1 and T2) of the electron spin (S), the electronic and proton g factors (g_e and g_N), the Bohr magneton (β), the distance between the nucleus and ion (r), the Larmor frequencies for proton and electron spins (ω_I and ω_S) and the correlations times τ_C and τ_e, corresponding to the molecular rotational correlation time and the internal rotational correlation time, respectively (GONÇALVES; PEIXOTO; DA CUNHA; RAMALHO, 2014).

These equations represent the relaxation rates, R1 and R2, respectively. R1 and R2 show the dependence of the dipolar coupling, where the first term in the sum, and the scalar coupling, is the second term in the sum (GONÇALVES; PEIXOTO; DA CUNHA; RAMALHO, 2014). The use of relaxation parameters is heavily applied for the investigation of MRI probes, which will be discussed in the next section.

The hyperfine coupling constant (A), will be one spectroscopic parameter explored in this work. It can be divided into isotropic (HFCC or A_{iso}) and anisotropic coupling constants (ASD), which have three contributions A_{xx}, $A_{yy,}$ and A_{zz}, where the sum of these contributions is null (BÜHL; IMHOF; REPISKY, 2004). The isotropic coupling constant is a contact interaction originating from the displacement of the unpaired electron over the nucleus. The anisotropic coupling constant is the electron-nucleus spin dipole interaction (KARUNAKARAN; BALAMURUGAN, 2018; OLIVEIRA; GUIMARÃES, 2000).

The main contributor to the hyperfine coupling constant is the isotropic interaction (A_{iso}). This constant of a nucleus is related to the spectral line spacing, which represents the difference between two peaks in a row and is measured in MHz, as can be seen in Figure 1 (FRECUS; RINKEVICIUS; ÅGREN, 2013).

Figure 1 – EPR spectrum. The hyperfine coupling, A, is highlighted.

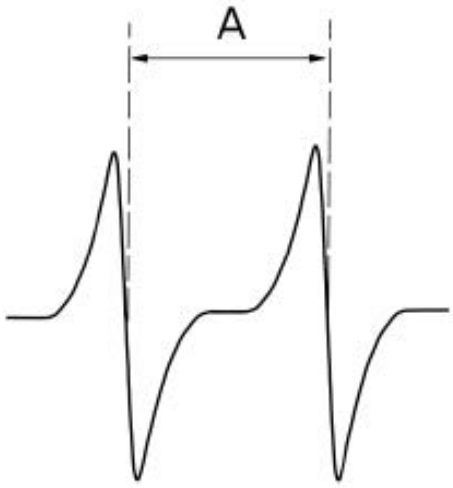

Reference: FRECUS; RINKEVICIUS; ÅGREN (2013).

2.2.2. Magnetic Resonance Imaging

Magnetic Resonance Imaging (MRI) techniques are based on the NMR principles, where a magnetic field was used to obtain data from the spin nuclei. In the MRI, those data are used to obtain an image that was formed from the distance between the protons of the sample or body and the magnetic field gradient (SKOOG; HOLLER; CROUCH, 2017).

This technique is often applied to hydrogen nuclei, so the image is obtained from the position of the hydrogen atoms in the tissue, usually coming from water or lipids molecules. To form the image, a B_0 was applied in each axis of the cartesian system, then by calculating the distance in axis x, y, and z between the spin and the source of the magnetic field, obtained a tridimensional data set with the voxel, that corresponds a set of x, y and z coordinates. This matrix of data allows the formation of images (D'ANJOU, 2017; SKOOG; HOLLER; CROUCH, 2017).

But these images are not always good in quality and definition, so compounds called contrast agents are used to improve the images, allowing a better view of the tissue and more precise diagnosis (WAHSNER; GALE; RODRÍGUEZ-RODRÍGUEZ; CARAVAN, 2019).

2.2.2.1.Contrast Agents

Contrast agents (CA's) are paramagnetic compounds used to decrease the longitudinal or transversal relaxation time of the water molecules, providing better quality images on MRI. CA's have an important role in the diagnosis by MRI (GONÇALVES; PEIXOTO; DA CUNHA; RAMALHO, 2014; PEREIRA; SILVA; GONÇALVES; MANCINI *et al.*, 2017; WAHSNER; GALE; RODRÍGUEZ-RODRÍGUEZ; CARAVAN, 2019).

The most used CA´s are based on Gadolinium (III) complexes, which correspond to about 40% of all CA's administration worldwide (WAHSNER; GALE; RODRÍGUEZ-RODRÍGUEZ; CARAVAN, 2019). These structures show a good performance to improve the quality of the images and often are applied associated with other substances that act as target molecules, focusing on specific areas of the body (PEREIRA; SILVA; GONÇALVES; MANCINI *et al.*, 2017; WAHSNER; GALE; RODRÍGUEZ-RODRÍGUEZ; CARAVAN, 2019).

Recently, however, several diseases were associated with CA's, and its permanence in the body was very long, leading to a search for new CA's based on different metallic centers with lower risk (WAHSNER; GALE; RODRÍGUEZ-RODRÍGUEZ; CARAVAN, 2019). The development of new CA's seeks the ability of this species to act in specific areas by itself, without the need for a target vector to localize the agent to a specific protein or cell type.

(DUFFY; HARBECK; NAP; MOLINA *et al.*, 2017; WAHSNER; GALE; RODRÍGUEZ-RODRÍGUEZ; CARAVAN, 2019).

These kinds of CA's are called biochemically targeted agents, which are designed to bind specifically to certain molecular targets, like proteins. Several new compounds have been designed for this purpose, like new Gd-based and Mn-based compounds (PEREIRA; SILVA; GONÇALVES; MANCINI *et al.*, 2017; WAHSNER; GALE; RODRÍGUEZ-RODRÍGUEZ; CARAVAN, 2019), magnetic iron oxide particles (GONÇALVES; PEIXOTO; DA CUNHA; RAMALHO, 2014) and Pt-based (PEREIRA; GONÇALVES; MANCINI; KUCA *et al.*, 2019) as biochemically targeted agents also has been reported .

2.3. Tyrosine Kinase Enzyme

Protein kinases are responsible for the communication of intracellular control, regulation, and signal transduction. Thus, the knowledge of their action mechanism has been extensively studied due to their activities related to several diseases, such as asthma, diseases of the central nervous system, diabetes, and breast cancer (SILVA; HORTA; ALENCASTRO; PINTO, 2009).

Specifically, the tyrosine kinase enzyme is responsible for catalyzing protein phosphorylation from the 3'-hydroxyl group of ATP (Figure 2). Since these enzymes are part of the control of cell proliferation, their deregulation causes several changes in cell processes, which can cause several diseases. Thus, the study of this enzyme is important for the treatment of several diseases, such as breast cancer (GAUTAM; BANSKOTA; LEE; LEE *et al.*, 2018; MAYER; ARTEAGA, 2016; NAIR; CHUNG; SUN; TYAGI *et al.*, 2018).

Figure 2 – Reaction catalyzed by tyrosine kinase enzyme (TK).

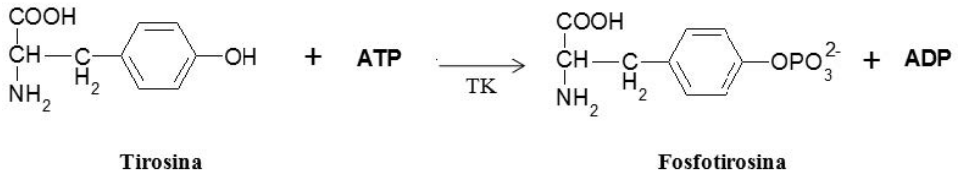

Reference: By the Author (2022).

The phosphoinositide 3-kinase (PI3K) enzyme is responsible for the growth of tumors, so its inhibition is a way of treating these diseases (JANKU, 2017). Just like other drugs, the search for inhibitors more powerful and less harmful to humans is constant. A family of compounds that is highlighted is derived from benzothiazoles, such as 2-(4-aminophenyl) benzothiazole, which has inhibitory properties against PI3K enzyme, when they compete for the ATP binding site in these enzymes (SHI; BRADSHAW; WRIGLEY; MCCALL *et al.*, 1996; YOU; YU; SUN; LUO *et al.*, 2017).

2.4. Benzothiazole and its derivates

Benzothiazoles are compounds formed with the reaction between o-iodoanilines and DMSO (Figure 3) (ZHU; ZHANG; KUANG; DENG *et al.*, 2020). This compound has a lot of derivatives, which have interesting pharmacological properties and they can be considered anti-cancer agents (MACHURA; WOLFF; BENOIST; COULAIS, 2013; MACHURA; WOLFF; GRYCA; PALION *et al.*, 2011; PEREIRA; GONÇALVES; MANCINI; KUCA *et al.*, 2019; PEREIRA; SILVA; GONÇALVES; MANCINI *et al.*, 2017; TZANOPOULOU; PIRMETTIS; PATSIS; PARAVATOU-PETSOTAS *et al.*, 2006; TZANOPOULOU; SAGNOU; PARAVATOU-PETSOTAS; GOURNI *et al.*, 2010).

Figure 3 – (a) Benzothiazole formation reaction. (b) Benzothiazole derivate 2-(4'-aminophenyl) benzothiazole.

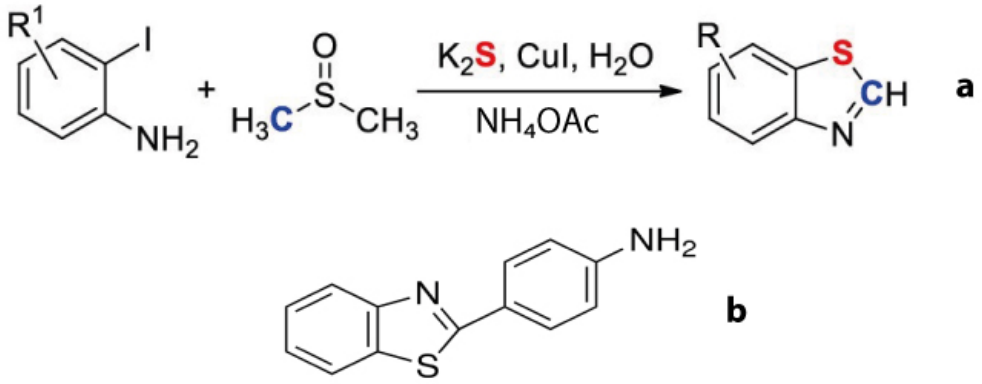

Reference: (a) Adapted from ZHU; ZHANG; KUANG; DENG *et al.* (2020). (b) By the Author (2022).

Among the benzothiazole derivates, phenilbenzothiazoles have high selectivity and proven anti-tumor activity (TZANOPOULOU; SAGNOU; PARAVATOU-PETSOTAS; GOURNI *et al.*, 2010). We can highlight the compound 2-(4'-aminophenyl) benzothiazole (Figure 3(b)), which has been reported as an anti-tumor agent (MAVROIDI; SAGNOU; STAMATAKIS; PARAVATOU-PETSOTAS *et al.*, 2016; PEREIRA; GONÇALVES; MANCINI; KUCA *et al.*, 2019; SHI; BRADSHAW; WRIGLEY; MCCALL *et al.*, 1996; TZANOPOULOU; SAGNOU; PARAVATOU-PETSOTAS; GOURNI *et al.*, 2010; YOU; YU; SUN; LUO *et al.*, 2017).

Several studies indicate Rhenium as a better candidate than the traditional ones, like Gadolinium, for use as a metallic center for CA's since it can be obtained easily and does not present radioactivity. In line with that, Re complexes conjugated with the compound 2-(4'-aminophenyl) benzothiazole (Figure 4) were synthesized to create stable complexes that can bind to specific receptors (TZANOPOULOU; PIRMETTIS; PATSIS; PARAVATOU-PETSOTAS *et al.*, 2006; TZANOPOULOU; SAGNOU; PARAVATOU-PETSOTAS; GOURNI *et al.*, 2010).

Figure 4 – $Re(CO)_3(NNO)$ conjugated to 2-(4'-aminophenyl) benzothiazole.

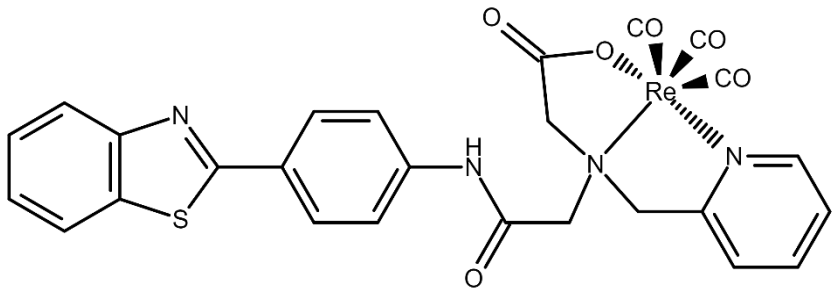

Reference: By the Author (2022)

2.5. Rhenium

Rhenium was discovered by the Germans Walter Noddack, Ida Tacke, and Otto Bergo in 1925, being the last naturally occurring chemical element found (SCERRI, 2010). They isolated the element, with atomic number 75 and atomic mass of 186.21u, from the mineral gadolinite. This metal has a silvery-white color and one of the highest melting points (3180 °C) and boiling point (5650 °C) (GREENWOOD; EARNSHAW, 2012).

Rhenium is in the third transition period, with electronic configuration $[Xe]6s^2 4f^{14} 5d^5$ and oxidation number varying between -1 and +7, with the most common Rhenium complexes being those with oxidation numbers +5, +3, and + 1. The complexes of Rhenium (I) and (V) are mostly diamagnetic, the latter of which may have a slight temperature-dependent paramagnetism. Abram, 2003, also reported that Re(III) complexes are predominantly paramagnetic, except for complexes with the coordination numbers of five or seven, which have diamagnetic properties (ABRAM, 2003; COLLERY; DESMAELE; VIJAYKUMAR, 2019; SIEH; KUBIAK, 2016).

The physicochemical characteristics of the Rhenium atom are varied, such as efficiency as a reducing agent (E_{0red}=0.300V) (GREENWOOD; EARNSHAW, 2012), resistance to high temperatures, good ductility, enabling different industrial applications of this metal (JOHN; SEAL II; POLYAK, 2017).

The two main radionuclides of Rhenium show a mass of 186 and 188u. The availability of $^{186|188}$Re allows them to be precursors of several radiopharmaceuticals, due to their proprieties of β-particle energy and their half-life. ^{188}Re, especially, shows high energy, about 2.11MeV, and shorter half-life, about 0.7 days, being more applicable to use as CA's for MRI (VOLKERT; HOFFMAN, 1999).

Complexes with Rhenium tricarbonyls core have been highlighted since the discovery of their photoluminescence properties discovered by Wrighton and Morse in the early 1970s (WRIGHTON; MORSE, 1974). Since then, several studies evaluating the ligands on the $[Re(CO)_3]$ core has been made for improving these properties for several applications (COLLERY; DESMAELE; VIJAYKUMAR, 2019; FAUSTINO; SOUZA; NUNES; DUONG *et al.*, 2018; MAŁECKA; MACHURA; ŚWITLICKA; KOTOWICZ *et al.*, 2020; SALOMÃO; GOMES; FERREIRA; MOURA *et al.*, 2019; SOUSA; SOUZA; BARROS; PATROCINIO, 2019).

In this contribution, we will highlight the complexes of Rhenium with phenilbenzothiazoles derivates that, as mentioned previously, have antitumor properties. These compounds are studied because of the physicochemical characteristics and relatively easy synthesis and high affinity to breast tumors, showing inhibitory activity to enzyme PI3K (MACHURA; WOLFF; BENOIST; COULAIS, 2013; TZANOPOULOU; PIRMETTIS;

PATSIS; PARAVATOU-PETSOTAS *et al.*, 2006; TZANOPOULOU; SAGNOU; PARAVATOU-PETSOTAS; GOURNI *et al.*, 2010).

Those complexes reveal promising applications for imaging detection and their inhibitory activity is confirmed by NMR ^{1}H and NMR ^{13}C (COLLERY; DESMAELE; VIJAYKUMAR, 2019; TZANOPOULOU; PIRMETTIS; PATSIS; PARAVATOU-PETSOTAS *et al.*, 2006; TZANOPOULOU; SAGNOU; PARAVATOU-PETSOTAS; GOURNI *et al.*, 2010). Machura and co-workers performed computational calculations and experiments considering synthesis and characterization of this family of complexes (MACHURA; WOLFF; BENOIST; COULAIS, 2013; MACHURA; WOLFF; GRYCA; PALION *et al.*, 2011). This type of study can help to elucidate the structural characteristics of rhenium complexes.

2.6. Computational Chemistry

Computational chemistry is generally divided into two major areas, molecular mechanics and quantum mechanics (CRAMER, 2013; JENSEN, 2017).

Molecular mechanics, also called classical methods, are based on Newton's principles and do not recognize the influence of the electronic structure of atoms in calculations. This group of techniques is widely used to study biological systems, for the development of new drugs, the action of a molecule in a specific enzyme, among other studies of macrosystems (CRAMER, 2013; JENSEN, 2017).

The quantum mechanics calculations include the effects of the electronic structure, where they solve the Schrödinger equation using approximations. This field can be divided into two different approaches, the semi-empirical methods, which solve the Schrödinger equation using parameters pre-defined by experimental data or other theoretical calculations, and the *ab-initio* calculations (CRAMER, 2013; JENSEN, 2017). These methods will be discussed in more detail in the next section.

2.6.1. Density Functional Theory

In the early 20th century several discoveries, including Einstein's and, especially, Schrödinger's equations, allowed a breakthrough in the relations of quantum mechanics. In equation 6 the Shrödinger equation is shown, where, ψ is the wave function, which despite not having a defined physical meaning, holds all information to determine the complete system, be it an atom, a molecule or a solid, and Ĥ is the Hamiltonian operator, which performs all operations capable of describing the system, either physically or its interactions.

$$\hat{H}\psi = E\psi \qquad (6)$$

The analytical resolution of the Schrödinger equation is only performed for monoelectronic systems, such as the hydrogen atom. The quantum *ab initio* methods, from Latin "since the beginning", were used to solve systems with a greater number of electrons, using the Hartree-Fock (HF) approximation. However, this approach fails to describe a fundamental characteristic for the investigation of the chemical properties of the system and the electronic correlation of molecular systems (CRAMER, 2013; PESSÔA; CORREIA; CARAUTA; SILVA, 2018).

The electronic correlation can be divided into two parts, the static electronic correlation (SEC) and the dynamic electronic correlation (DEC), which are treated as an approximation in the HF method, to solve this problem, the post-HF methods emerged. The *ab initio* post-HF methods used to explain SEC is called multiconfigurational methods (CAS, RAS, among others). They use Slater's determinants to describe the electronic configuration of the system's fundamental state, which in the HF method is described by only one Slater's determinant. However, more than one electronic configuration is needed to describe the fundamental state, since they can describe systems involving heavy atoms in which there is a crossing between energy levels (JENSEN, 2017).

Since the DEC corresponds to about 90% of the total electronic correlation of the system, most post-HF methods (CI, MP2, CCSD (T), among others) describe only this item, some methods, such as CASPT2, describe all the correlations of the system (JENSEN, 2017).

The big problem with post-HF calculations is the high computational demand. While the HF method has a computational cost that increases according to N^4, where N is the number of electrons in the system, post-HF methods are scaled with at least N^5, N^6, ..., N^n. To try to

mitigate this problem comes the density functional theory - DFT (CRAMER, 2013; JENSEN, 2017; MORGON, 2007).

Instead of the wave function, DFT is based on the adoption of the approximation of electronic density as the variable of the Schrödinger equation, known as the Thomas-Fermi method. They, working independently, used statistical models to approximate the electronics distribution of the system for its density, which corresponds to the square of the wave function (Equation 7). The density of the system has a clear physical meaning, it corresponds to the region where it is most likely to find electrons (JENSEN, 2017).

$$\rho(r) =< \psi|\psi > \qquad (7)$$

While the wave function of *N* electrons depends on 4 *N* (the cartesian coordinates *x*, *y,* and *z* and the electron spin coordinate), the electronic density (ρ) depends only on the cartesian coordinates *x*, *y,* and *z*, regardless of the number of electrons. Even though it is known that each ρ produces energy for the fundamental state, the functional that relate the electronic density and the real energy of the fundamental state was unknown until the 1960s when the Hohenberg-Kohn theorems emerged (JENSEN, 2017).

The ideas that underlie DFT arise from the two Hohenberg-Kohn (HK) theorems, which show, in general terms, that:

Theorem 1 - An external potential (V_{ext}(r)) for the electrons of the system, that is, the one that describes the nuclear interaction with the electrons, is determined solely by the density of the ground state so to describe the dependence on energy of the fundamental state concerning this density, it is enough to show that this density determines the Hamiltonian operator ($\hat{H}$) of the system and that its integration provides the number of electrons in the system (Equation 8) (DUARTE, 2001).

$$\int \rho(r) = N \qquad (8)$$

This theorem then establishes that the energy can be described in terms of a functional of the electronic density of the fundamental state. To corroborate with this result that a certain density is the density in the fundamental state, Theorem 2 establishes that:

Theorem 2 - The electronic density of the fundamental state can be calculated, in principle, using the variational method, where the total calculated energy of this density

(E[ρ(r)]) cannot be less than the real energy of the fundamental state (E_0), as shown in Equation 9. The name "functional" comes from the fact that energy depends on a function, which in DFT is density, which in turn depends on spatial variables, *i.e.*, E[ρ(**r**)]. In the case of wave function-based methods, energy is a function of the wave function (*E*[ψ(**r**)]) (DUARTE, 2001).

$$E[\rho(r)] \geq E_0 \qquad (9)$$

In both the HF and DFT methods, the Hamiltonian ($\hat{H}$) is time-independent and non-relativistic. This operator contains the terms of the kinetic energy of the nuclei and electrons and the terms of their electrostatic interactions (Equation 10).

$$\hat{H} = \hat{T}_N + \hat{T}_e + \hat{V}_{Ne} + \hat{V}_{NN} + \hat{V}_{ee} \qquad (10)$$

where the indexes N, corresponds to the nucleus, and *e* corresponds to electrons. All terms in the equation describe a part of the physical interactions existing in the system, presented in equations 11 to 15.

- Nuclear kinetic energy:

$$\hat{T}_N = -\sum_A \frac{1}{2M_A} \bar{V}_A^2 \qquad (11)$$

- Potential energy between nucleus:

$$\hat{V}_{NN} = \sum_A \sum_{B>A} \frac{Z_A Z_B}{|R_A - R_B|} \qquad (12)$$

- Electronic kinetic energy:

$$\hat{T}_e = -\sum_i \frac{1}{2} \bar{V}_i^2 \qquad (13)$$

- Potential energy between electrons:

$$\hat{V}_{ee} = \sum_i \sum_{j>i} \frac{1}{|r_i - r_j|} \qquad (14)$$

- Electron-nucleus potential energy:

$$\hat{V}_{Ne} = -\sum_i \sum_A \frac{Z_A}{|R_A - r_i|} \qquad (15)$$

In both methods, the Born-Oppenheimer approach is applied, which separates the nuclear movement from the electronic movement. This is only possible due to the large

difference in mass between electrons and nucleus, providing an almost immediate adaptation to different nuclear dispositions. Thus, the term nuclear kinetic energy of *H* is null and the term electron-nucleus potential energy is a constant (JENSEN, 2017).

We can express the energy of the fundamental electronic state according to equation 16, applying the HK theorems.

$$E_0 \leq E[\rho(r)] = T_e[\rho_0] + E_{ee}[\rho_0] + E_{Ne}[\rho_0] \qquad (16)$$

However, the HK theorems do not provide enough information for the construction of the density functionalities mentioned above. Only the functional $E_{Ne}[\rho_0]$ is fully known. With this in mind, there is the development of the Kohn-Sham (KS) method, which makes the direct application of these theorems in atomic and molecular systems viable (DUARTE, 2001; KOHN, 1965).

In this method, the density of a fictional system with electrons that do not interact can be considered as a representation of the density of the fundamental state of a real system. The kinetic part of the fictitious system is similar to the kinetic part of the HF method, so a correction term is added to the kinetic energy functional (Equation 17).

$$T[\rho] = T_s[\rho] + T_c[\rho] \qquad (17)$$

where $T_s[\rho]$ is the kinetic energy of a fictitious system and $T_c[\rho]$ is the kinetic correction due to electron-electron interaction. The contribution of $T_c[\rho]$ is small when compared to $T_s[\rho]$.

The exact density functional for Coulomb's classic part of the interaction of two electrons (Equation 18), however, it is necessary to know the non-classical electron-electron interactions, often known as exchange and correlation interactions.

$$J[\rho] = \iint \frac{\rho x_1 + \rho x_2}{r_{12}} \delta x_1 \delta x_2 \qquad (18)$$

In the KS method, the exchange and correlation interactions are inserted into an approximate functional, called the exchange and correlation functional (Equation 19).

$$E_{xc}[\rho] = E_x[\rho] + E_c[\rho] + T_c[\rho] \qquad (19)$$

Thus, the total electronic energy can be expressed according to equation 20.

$$E_{elect}[\rho] = T_s[\rho] + \int V_{ext}\rho(x) + J[\rho] + E_{xc}[\rho] \qquad (20)$$

The exact expression for the exchange and correlation functional is not known, so for the use of the KS method, an appropriate determination of the exchange and correlation term is necessary. This term presents the most difficult physical interpretation of DFT. To perform the approximations, the local density approximation (LDA) and the generalized gradient approximation (GGA) are usually used (DUARTE, 2001; JENSEN, 2017).

The development of this exchange and correlation function has been studied to advance DFT. The first step towards this is the complete understanding of the chemical characteristics of the system to be investigated. Since there are several functionals available for DFT calculations, this understanding provides a better choice for the functional to be employed (JENSEN, 2017).

Despite a large number of functionals available, problems still exist, and knowing them is important to improve computational investigations. The first problem is known as asymptotic behavior, where chemical properties involving differences in orbital energies, ionization energy, electron-affinity, among others are not adequately described, in molecular systems containing an electron located far from the nucleus, which will be shielded by the other electrons, when comparing the experimental values (JENSEN, 2017).

Another known problem with DFT is called derived discontinuity. None of the available functionalities can describe the potential for exchange and correlation with the variation in the number of electrons, a phenomenon that reflects the chemical potential for charge transfer between two systems (JENSEN, 2017).

The last problem is called electron self-interaction, which occurs when there is no total cancellation of the exchange and correlation functional self-interaction part with the corresponding part of Coulomb interactions, causing errors to appear when applied to paramagnetic systems (JENSEN, 2017).

These three problems do not occur in the HF method, therefore, the use of hybrid functionalities, which consider the HF method to correct the problems with DFT, has been a widely used solution (JENSEN, 2017).

2.6.2. Relativistic Effects

Well-known characteristics of several compounds are explained by the relativistic effects, such as the yellow color of Gold, the liquid Mercury at room temperature, and the major part of the voltage of the lead-acid battery (PYYKKÖ, 2012). Heavy elements, such as Rhenium, are greatly influenced by the relativistic effects in their properties and compounds (PYYKKÖ, 2012; ZÚÑIGA; OYARZÚN; MARTIN-TRANSACO; YÁÑEZ-S *et al.*, 2017).

So, the inclusion of these phenomena in quantum calculations, especially for compounds with heavy elements, is crucial. To provide this inclusion, the relativistic effects are added on the Hamiltonian, with several different implementations available, but they all stem from the generic form of the electronic Hamiltonian within the Born-Oppenheimer approximation (Equation 21).

$$\hat{H} = \sum_i \hat{h}\,(i) + \frac{1}{2}\sum_{i \neq j} \hat{g}(i,j) + V_{NN}\,, \qquad (21)$$

where $\hat{h}$ is the one-electron operator, $\hat{g}$ is the two-electron operator, and V_{NN} is the classical repulsion of clamped nuclei.

Usually, the relativistic effects are split into two contributions, being the first, the spin-orbit coupling (SO) interactions, that are the relativistic effects in many-electron systems provided by the electron-electron interactions, and, the second, the scalar relativistic (SR) effects, that came from the relativistic effects at the one-electron level. Different methods are available for quantum chemical calculations considering fully and quasi-relativistic approaches, one of the most well-known is all-electron that considers in the Hamiltonian only SR terms or both SR and SO, being, ideally, more accurate than the first one (AUTSCHBACH; ZHENG, 2009).

One of the limiting factors for working with quantum chemical calculations considering the relativistic effects is the computational cost that increases, independent of the size of the system. This occurs as a result of the fully relativistic Dirac Hamiltonian, which is a 4 x 4 matrix operator, while the non-relativistic one-electron is a scalar operator. The Dirac Hamiltonian includes the spin explicitly and describes the electron and the positron, which leads to an increase of the dimension of the one-electron wave function, *i.e.* the orbitals (SAUE, 2011).

The Dirac equation was the initial point for the relativistic quantum chemistry, being essential for the study of relativistic quantum mechanics and quantum electrodynamics, which performs the conversion of the classical relativistic energy-momentum relation (Equation 22) (SAUE, 2011):

$$E = \sqrt{c^2p^2 + m^2c^4} \qquad (22)$$

To get the relativistic Hamiltonian for a free particle the momentum *p* was replaced for the differential operator -*iħ*Δ, leading to Equation 23 (SAUE, 2011):

$$H = \sqrt{-c^2\hbar^2\Delta + m^2c^4} \qquad (23)$$

Now, the time-dependency of the Dirac equation can be described in the Schrödinger form (Equation 24) (SAUE, 2011):

$$i\hbar\frac{d}{dt}(t, \boldsymbol{x}) = H_0\psi(t, \boldsymbol{x}), \qquad \psi(t_0, \boldsymbol{x}) = \psi(\boldsymbol{x}) \qquad (24)$$

Dirac realized that his equation (Equation 22) could be linearized, getting the Dirac operator for free particles (Equation 25), by introducing matrices (SAUE, 2011).

$$H_0 = \sqrt{c^2p^2 + m^2c^4} = c\boldsymbol{\alpha}.\boldsymbol{p} + \boldsymbol{\beta}mc^2, \qquad (25)$$

where the momentum $\boldsymbol{p} = -i\hbar\nabla$ is the differential operator and the operators $\boldsymbol{\alpha}$ and $\boldsymbol{\beta}$ are the Dirac 4 x 4 matrices (Equation 26):

$$\boldsymbol{\alpha} = \begin{pmatrix} 0_2 & \boldsymbol{\sigma} \\ \boldsymbol{\sigma} & 0_2 \end{pmatrix}; \ \boldsymbol{\beta} = \begin{pmatrix} I_2 & 0_2 \\ 0_2 & -I_2 \end{pmatrix} \qquad (26)$$

where 0_2 is the 2 x 2 zero matrix, $\boldsymbol{\sigma}(\boldsymbol{\sigma} = \sigma_x, \sigma_y, \sigma_z)$ are the 2 x 2 Pauli spin matrices and I_2 is the 2 x 2 identity matrix. After rearranging the Dirac equation, we have equation 27, which is the Dirac equation in an external field (VAN LENTHE; BAERENDS; SNIJDERS, 1994).

$$H^D\Psi^D = \begin{pmatrix} V & c\boldsymbol{\sigma}.\boldsymbol{p} \\ c\boldsymbol{\sigma}.\boldsymbol{p} & V - 2c^2 \end{pmatrix} = E\Psi^D \qquad (27)$$

The influence of the external field is included in the kinetic energy H_0 and is described by the potential energy V(x). Equation 28 shows the operator H^D, which describes the energy of a particle in an external field.

$$H^D = H_0 + V(x) \qquad (28)$$

Equation 25 could present two possible results, one positive and one negative energy, which is called positron and usually is neglected in non-relativistic calculations, and it is common to call them orbitals or 1-component 1-electron wavefunctions. The search for a solution to the negative energy is an object of research in quantum chemistry and the solution for the Dirac equation is a four-component vector.

The eigenvector solutions of the 4 x 4 matrix form of Equation 25 are composed of four components as shown in Equation 29 (AUTSCHBACH, 2012).

$$\Psi^D = \begin{pmatrix} \psi_1 \\ \psi_2 \\ \psi_3 \\ \psi_4 \end{pmatrix} = \begin{pmatrix} \psi_L \\ \psi_S \end{pmatrix}; \qquad (29)$$

$$\psi_L = \begin{pmatrix} \psi_1 \\ \psi_2 \end{pmatrix}, \quad \psi_S = \begin{pmatrix} \psi_3 \\ \psi_4 \end{pmatrix}$$

The eigenvector solution of the Dirac wave function is split into two components, the large (ψ_L) and the small (ψ_S). For the positive energy solutions, the large component has a large amplitude, while the small component has a small amplitude. When it is considered a free particle, i.e., $V = 0$ for all *r*, in the solution of the Dirac equation, two different results are obtained. The first one is the solutions with eigenvalues greater than $+mc^2$ and the second result with eigenvalues less than $-mc^2$. The positive solutions are of interest to quantum chemistry.

For this solution, the large component contributions are much larger than the small component. The combination of equations 27 and 29 lead us to the following expressions:

$$V\psi_L + c\boldsymbol{\sigma}.\boldsymbol{p}\psi_S = E\psi_L \qquad (30)$$

$$c\boldsymbol{\sigma}.\boldsymbol{p}\psi_L + (V - 2c^2)\psi_S = E\psi_S \qquad (31)$$

Now, with equations 30 and 31, the large and small components of the Dirac wave function could be joined by the following equations.

$$\psi_S = \frac{1}{2c} k\boldsymbol{\sigma}.\boldsymbol{p}\psi_L \qquad (32)$$

$$k = \left(1 - \frac{V - E}{2c^2}\right)^{-1} \qquad (33)$$

These equations could eliminate the small component of the Dirac wave function and points solutions just for the large component, this approach leads to an eigenvalue equation for the large component.

$$\left[V + \frac{1}{2}\boldsymbol{\sigma}.\boldsymbol{p}k\boldsymbol{\sigma}.\boldsymbol{p}\right]\psi_L = E\psi_L \qquad (34)$$

However, this equation is not usable once the Hamiltonian operator is related to *k* (and *E*). To split the large and small components completely, the Foldy-Wouthuysen transformations (FOLDY; WOUTHUYSEN, 1950) can be used, leading to an exact two-component relativistic method. Another approach leads to quasi-relativistic two-component methods, which consist to split the components using an expansion of k in a power series. Probably, the most famous example of this approach is the Zeroth Order Regula Approximation, ZORA (VAN LENTHE; BAERENDS; SNIJDERS, 1994; VAN LENTHE; VAN LEEUWEN; BAERENDS; SNIJDERS, 1996; VAN LENTHE; SNIJDERS; BAERENDS, 1996).

The expansion of k leads to equation 35, which is a more useful equation for the Hamiltonian in equation 34.

$$k = \left(1 - \frac{V-E}{2c^2}\right)^{-1} = 1 + \sum_{n=1}^{\infty}\left(\frac{V-E}{2c^2}\right)^n \qquad (35)$$

After some manipulations, the Pauli Hamiltonian is obtained at the first order of this expansion.

$$H^{Pauli} = V + \frac{p^2}{2} - \frac{p^4}{8C^2} + \frac{Vp^2}{8c^2} + \frac{i}{4c^2}\boldsymbol{\sigma}.(\boldsymbol{\nabla}V \times \boldsymbol{p}) \qquad (36)$$

The first and the second term of equation 36 are related to the non-relativistic Hamiltonian; the third term is the mass-velocity operator, which considers the relativistic corrections to the kinetic energy related to the increase of the mass in special relativity; the fourth term is the Darwin term, which includes the correction to the potential near the nucleus; the fifth term is the spin-orbit coupling term.

A different expansion could be used for k by the following expression (Equation 37) (VAN LENTHE; VAN LEEUWEN; BAERENDS; SNIJDERS, 1996):

$$k = \frac{c^2}{2c^2 - V}\left(1 + \frac{E}{2c^2 - V}\right)^{-1}$$

$$= \frac{c^2}{2c^2 - V} + \left(\frac{c^2}{2c^2 - V}\right)\sum_{n=1}^{\infty} -1^n \left(\frac{E}{2c^2 - V}\right)^n \quad (37)$$

After some rearrangements, the ZORA Hamiltonian can be obtained, at the zeroth order of this expansion series (Equation 38).

$$H^{ZORA} = V + \frac{1}{2}\boldsymbol{\sigma}.\boldsymbol{p}\left(\frac{c^2}{2c^2 - V}\right)\boldsymbol{\sigma}.\boldsymbol{p}$$

$$= V + \frac{1}{2}\boldsymbol{p}\left(\frac{c^2}{2c^2 - V}\right)\boldsymbol{p} + \frac{i}{2}\left(\frac{c^2}{2c^2 - V}\right)^2 \boldsymbol{\sigma}.(\boldsymbol{\nabla} V \times \boldsymbol{p}) \quad (38)$$

The ZORA implementation is a two-component method when the spin-orbit coupling is included and a one-component method when only scalar-relativistic effects are considered. The ZORA Hamiltonian produces valence-shell properties and orbital energies of heavy elements, as can four-component relativistic methods (VAN LENTHE; VAN LEEUWEN; BAERENDS; SNIJDERS, 1996).

ZORA method could be used to simulate most of the relativistic effects, including when heavy elements are present, and show a good cost-benefit as an alternative to the 4-component Dirac-Coulomb (DC) Hamiltonian.

2.6.3. Molecular Docking

This technique is widely used for the designing of new compounds with biological activity; playing an important role in discovering the way a small molecule, usually, an inhibitor, called ligand, interacts with the active site of a molecular target, called receptor. To define this, the interactions are calculated, including the Coulombic interactions, van dew Waals interactions, and the formation of hydrogen bonds (PAGADALA; SYED; TUSZYNSKI, 2017).

There are three main types of molecular docking, rigid body docking, semi-rigid docking, and flexible docking (PAGADALA; SYED; TUSZYNSKI, 2017). On rigid body docking, the ligand has conformational freedom and the receptor are frozen. The flexible

docking allowed all species present in the system to be kept free. The semi-rigid docking, on the other hand, maintains the freedom of the ligand and allows some residues of the receptor to remain free (PAGADALA; SYED; TUSZYNSKI, 2017).

They are based on three different models, lock-and-key, induced-fit and conformational selection. These models seek to explain how the binding mechanism of ligand-receptor occurs. The first one happens when the ligand (key) has the exact size to bind to the receptor (lock), this model does not consider the conformational variability of the protein. The induced-fit model appears to fill the gaps left by the key-and-lock model, and takes the receptor as flexible, leading to a change in the ligand conformation to fit in the active site, taking the conformation variability of the bonding, i.e., the conformation variability arises in the presence of the ligand (DU; LI; XIA; AI *et al.*, 2016).

However, these two models consider the receptor as rigid after the binding, but most proteins are inherently dynamic, i.e., the conformation variability is independent of the ligand, so there are several different conformations and those where the ligand is most likely to bind are preferred. Thus, the conformational selection model arises using modern theories to explain the binding mode of ligand-receptor (DU; LI; XIA; AI *et al.*, 2016). An illustration of these three models can be seen in Figure 5.

Figure 5 – Schematic illustrations of the three protein-ligand binding models: (a) Lock-and-key; (b) Induced fit; and (c) Conformational selection.

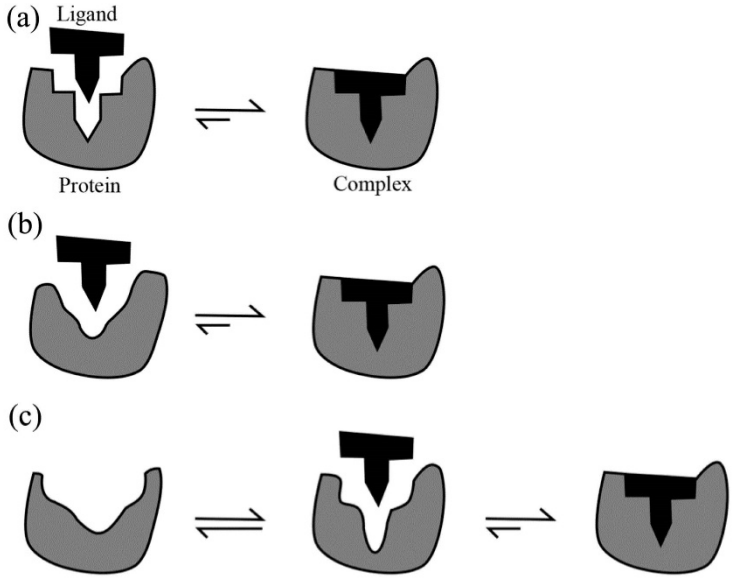

Reference: DU; LI; XIA; AI *et al.* (2016).

This computational method is widely used once they provide a good prediction of the complex formed by the ligand-receptor binding (MENG; ZHANG; MEZEI; CUI, 2011).

3. GENERAL CONCLUSIONS

In this research, rhenium complexes of 2-(4'-aminophenyl) benzothiazole (ReABT) were studied to purpose as an alternative in breast cancer diagnosis. This work was divided into two parts, the first one, ReABT was evaluated as a potential spectroscopic probe in magnetic resonance image (MRI) using EPR parameters through DFT calculations. The second part was dedicated to studying the ReABT complex as a probe using ^{187}Re shielding tensors performing NMR calculations through GIAO-DFT methods. These calculations were performed in three different chemical environments: gas phase, implicit solvent, and inside the active site ok PI3K enzyme.

Once the relativistic effects are pronounced on Rhenium, the ZORA implementation, both in the Hamiltonian and Basis Set, were used to analyze the importance of these effects on the EPR and NMR calculations. These results point out that for both cases the relativistic effects are important, being closer to the reference values when compared to non-relativistic calculations.

Rhenium compounds for application as a spectroscopic probe are, in general, less toxic than traditionally gadolinium-based compounds applied for breast cancer diagnosis. In this context, the ReABT complex exhibits potential for application as a spectroscopic probe for breast cancer diagnosis. Thus, the study of this complex is important to help the development of new effective and less toxic compounds for breast cancer diagnosis. Therefore, this research sheds light on the importance of studying EPR and NMR parameters of ReABT, as well as, the best protocols to perform these calculations. Thus, experimental studies using the ReABT complex will be an important step for the sequence of this work.

REFERENCES

ABRAM, U. 5.3 - Rhenium. *In*: MCCLEVERTY, J. A. e MEYER, T. J. (Ed.). **Comprehensive Coordination Chemistry II**. Oxford: Pergamon, 2003. p. 271-402.

AUTSCHBACH, J. Perspective: relativistic effects. **The Journal of chemical physics**, 136, n. 15, p. 150902, 2012.

AUTSCHBACH, J.; ZHENG, S. Relativistic computations of NMR parameters from first principles: theory and applications. **Annual Reports on NMR Spectroscopy**, 67, p. 1-95, 2009.

BARBA, D.; LEÓN-SOSA, A.; LUGO, P.; SUQUILLO, D. *et al.* Breast cancer, screening and diagnostic tools: All you need to know. **Critical Reviews in Oncology/Hematology**, 157, p. 103174, 2021/01/01/ 2021.

BÜHL, M.; IMHOF, P.; REPISKY, M. Rovibrational Corrections to Transition Metal NMR Shielding Constants. **ChemPhysChem**, 5, n. 3, p. 410-414, 2004/03/19 2004. https://doi.org/10.1002/cphc.200300979.

CARNEIRO, A. A. O.; VILELA, G. R.; DE ARAUJO, D. B.; BAFFA, O. MRI relaxometry: methods and applications. **Brazilian journal of physics**, 36, n. 1A, p. 9-15, 2006.

COLLERY, P.; DESMAELE, D.; VIJAYKUMAR, V. Design of Rhenium compounds in targeted anticancer therapeutics. **Current pharmaceutical design**, 25, n. 31, p. 3306-3322, 2019.

CRAMER, C. J. **Essentials of computational chemistry: theories and models**. John Wiley & Sons, 2013. 1118712277.

DU, X.; LI, Y.; XIA, Y.-L.; AI, S.-M. *et al.* Insights into Protein–Ligand Interactions: Mechanisms, Models, and Methods. **International Journal of Molecular Sciences**, 17, n. 2, 2016.

DUARTE, H. A. Índices de reatividade química a partir da teoria do funcional de densidade: formalismo e perspectivas. **Química Nova**, 24, n. 4, p. 501-508, 2001.

DUFFY, M. J.; HARBECK, N.; NAP, M.; MOLINA, R. *et al.* Clinical use of biomarkers in breast cancer: Updated guidelines from the European Group on Tumor Markers (EGTM). **European journal of cancer**, 75, p. 284-298, 2017.

D'ANJOU, M.-A. Principles of computed tomography and magnetic resonance imaging. **Textbook of Veterinary Diagnostic Radiology-E-Book**, 71, 2017.

FAUSTINO, L. A.; SOUZA, B. L.; NUNES, B. N.; DUONG, A.-T. *et al.* Photocatalytic CO2 reduction by Re (I) polypyridyl complexes immobilized on niobates nanoscrolls. **ACS Sustainable Chemistry & Engineering**, 6, n. 5, p. 6073-6083, 2018.

FOLDY, L. L.; WOUTHUYSEN, S. A. On the Dirac theory of spin 1/2 particles and its non-relativistic limit. **Physical Review**, 78, n. 1, p. 29, 1950.

FRECUS, B.; RINKEVICIUS, Z.; ÅGREN, H. π-Stacking effects on the EPR parameters of a prototypical DNA spin label. **Physical Chemistry Chemical Physics**, 15, n. 25, p. 10466-10471, 2013. 10.1039/C3CP51129D.

GALVÃO, E.; MARTINS, L. M. S.; IBIAPINA, J. O.; ANDRADE, H. M. *et al.* Breast cancer proteomics: a review for clinicians. **Journal of cancer research and clinical oncology**, 137, n. 6, p. 915-925, 2011.

GAUTAM, J.; BANSKOTA, S.; LEE, H.; LEE, Y.-J. *et al.* Down-regulation of cathepsin S and matrix metalloproteinase-9 via Src, a non-receptor tyrosine kinase, suppresses triple-negative breast cancer growth and metastasis. **Experimental & molecular medicine**, 50, n. 9, p. 1-14, 2018.

GONÇALVES, M. A.; PEIXOTO, F. C.; DA CUNHA, E. F. F.; RAMALHO, T. C. Dynamics, NMR parameters and hyperfine coupling constants of the Fe3O4(100)–water interface: Implications for MRI probes. **Chemical Physics Letters**, 609, p. 88-92, 2014/08/05/ 2014.

GREENWOOD, N. N.; EARNSHAW, A. **Chemistry of the Elements**. Elsevier, 2012. 0080501095.

HE, Z.; CHEN, Z.; TAN, M.; ELINGARAMI, S. *et al.* A review on methods for diagnosis of breast cancer cells and tissues. **Cell Proliferation**, 53, n. 7, p. e12822, 2020/07/01 2020. https://doi.org/10.1111/cpr.12822.

INCA. Instituto Nacional de Câncer José Alencar Gomes da Silva. Estimativa 2018: Incidência de Câncer no Brasil. Rio de Janeiro. INCA RJ 2019.

JAFARI, S. H.; SAADATPOUR, Z.; SALMANINEJAD, A.; MOMENI, F. *et al.* Breast cancer diagnosis: Imaging techniques and biochemical markers. **Journal of cellular physiology**, 233, n. 7, p. 5200-5213, 2018.

JANKU, F. Phosphoinositide 3-kinase (PI3K) pathway inhibitors in solid tumors: From laboratory to patients. **Cancer Treatment Reviews**, 59, p. 93-101, 2017/09/01/ 2017.

JENSEN, F. **Introduction to computational chemistry**. John wiley & sons, 2017. 1118825993.

JOHN, D. A.; SEAL II, R. R.; POLYAK, D. E. **Rhenium**. Reston, VA, p. 62. 2017. (1802P).

KARUNAKARAN, C.; BALAMURUGAN, M. Chapter Four - Electron Paramagnetic Resonance Spectroscopy. *In*: KARUNAKARAN, C. (Ed.). **Spin Resonance Spectroscopy**: Elsevier, 2018. p. 169-228.

KOHN, W. Time-dependent Kohn–Sham density-functional theory. **Physical Review A**, 1133, p. 140-148, 1965.

MACHURA, B.; WOLFF, M.; BENOIST, E.; COULAIS, Y. Tricarbonyl rhenium(I) complex of benzothiazole – Synthesis, spectroscopic characterization, X-ray crystal structure and DFT calculations. **Journal of Organometallic Chemistry**, 724, p. 82-87, 2013/01/15/ 2013.

MACHURA, B.; WOLFF, M.; GRYCA, I.; PALION, A. *et al.* Novel Re(I) tricarbonyl complexes of chelating ligands with aromatic N-heterocycle ring and aliphatic amine donor – Synthesis, spectroscopic characterization, X-ray structure and DFT calculations. **Polyhedron**, 30, n. 13, p. 2275-2285, 2011/08/23/ 2011.

MAVROIDI, B.; SAGNOU, M.; STAMATAKIS, K.; PARAVATOU-PETSOTAS, M. *et al.* Palladium (II) and platinum (II) complexes of derivatives of 2-(4′-aminophenyl) benzothiazole as potential anticancer agents. **Inorganica Chimica Acta**, 444, p. 63-75, 2016.

MAYER, I. A.; ARTEAGA, C. L. The PI3K/AKT pathway as a target for cancer treatment. **Annual review of medicine**, 67, p. 11-28, 2016.

MAŁECKA, M.; MACHURA, B.; ŚWITLICKA, A.; KOTOWICZ, S. *et al.* Towards better understanding of photophysical properties of rhenium(I) tricarbonyl complexes with terpy-like ligands. **Spectrochimica Acta Part A: Molecular and Biomolecular Spectroscopy**, 231, p. 118124, 2020/04/15/ 2020.

MENG, X.-Y.; ZHANG, H.-X.; MEZEI, M.; CUI, M. Molecular docking: a powerful approach for structure-based drug discovery. **Current computer-aided drug design**, 7, n. 2, p. 146-157, 2011.

MORGON, N. H. **Métodos de química teórica e modelagem molecular**. Editora Livraria da Física, 2007. 858832587X.

NAIR, A.; CHUNG, H.-C.; SUN, T.; TYAGI, S. *et al.* Combinatorial inhibition of PTPN12-regulated receptors leads to a broadly effective therapeutic strategy in triple-negative breast cancer. **Nature medicine**, 24, n. 4, p. 505, 2018.

OLIVEIRA, I. S.; GUIMARÃES, A. P. Interações hiperfinas. **Revista Brasileira de Ensino de Física**, 22, n. 3, p. 353-359, 2000.

PAGADALA, N. S.; SYED, K.; TUSZYNSKI, J. Software for molecular docking: a review. **Biophysical reviews**, 9, n. 2, p. 91-102, 2017.

PAVIA, D. L.; LAMPMAN, G. M.; KRIZ, G. S.; VYVYAN, J. R. **Introdução à espectroscopia**. Cengage Learning, 2010. 8522107084.

PEREIRA, B. T. L.; GONÇALVES, M. A.; MANCINI, D. T.; KUCA, K. *et al.* First Attempts of the Use of 195Pt NMR of Phenylbenzothiazole Complexes as Spectroscopic Technique for the Cancer Diagnosis. **Molecules**, 24, n. 21, p. 3970, 2019.

PEREIRA, B. T. L.; SILVA, É. F.; GONÇALVES, M. A.; MANCINI, D. T. *et al.* Exploring EPR Parameters of ⁹⁹Tc Complexes for Designing New MRI Probes: Coordination Environment, Solvent, and Thermal Effects on the Spectroscopic Properties. **Journal of Chemistry**, 2017, p. 8102812, 2017/06/14 2017.

PESSÔA, K. F.; CORREIA, J. C. G.; CARAUTA, A. N. M.; SILVA, F. B. D. Revisão de alguns principais métodos utilizados em modelagem molecular. Parte II-Métodos quânticos. 2018.

PYYKKÖ, P. Relativistic effects in chemistry: more common than you thought. **Annual review of physical chemistry**, 63, p. 45-64, 2012.

SALOMÃO, P. E. A.; GOMES, D. S.; FERREIRA, E. J. C.; MOURA, F. *et al.* Photoelectrochemical hydrogen production from water splitting using heterostructured nanowire arrays of Bi2O3/BiAl oxides as a photocathode. **Solar Energy Materials and Solar Cells**, 194, p. 276-284, 2019.

SAUE, T. Relativistic Hamiltonians for chemistry: A primer. **ChemPhysChem**, 12, n. 17, p. 3077-3094, 2011.

SCERRI, E. Recognizing rhenium. **Nature Chemistry**, 2, n. 7, p. 598-598, 2010/07/01 2010.

SHI, D.-F.; BRADSHAW, T. D.; WRIGLEY, S.; MCCALL, C. J. *et al.* Antitumor Benzothiazoles. 3. Synthesis of 2-(4-Aminophenyl)benzothiazoles and Evaluation of Their Activities against Breast Cancer Cell Lines in Vitro and in Vivo. **Journal of Medicinal Chemistry**, 39, n. 17, p. 3375-3384, 1996/01/01 1996.

SIEH, D.; KUBIAK, C. P. A Series of Diamagnetic Pyridine Monoimine Rhenium Complexes with Different Degrees of Metal-to-Ligand Charge Transfer: Correlating 13C

NMR Chemical Shifts with Bond Lengths in Redox-Active Ligands. **Chemistry–A European Journal**, 22, n. 30, p. 10638-10650, 2016.

SILVA, B. V.; HORTA, B. A. C.; ALENCASTRO, R. B. D.; PINTO, A. C. Proteínas quinases: características estruturais e inibidores químicos. **Quimica nova**, 32, n. 2, p. 453-462, 2009.

SKOOG, D. A.; HOLLER, F. J.; CROUCH, S. R. **Principles of instrumental analysis**. Cengage learning, 2017. 1337468037.

SOUSA, S. F.; SOUZA, B. L.; BARROS, C. L.; PATROCINIO, A. O. T. Inorganic Photochemistry and Solar Energy Harvesting: Current Developments and Challenges to Solar Fuel Production. **International Journal of Photoenergy**, 2019, 2019.

TZANOPOULOU, S.; PIRMETTIS, I. C.; PATSIS, G.; PARAVATOU-PETSOTAS, M. *et al.* Synthesis, characterization, and biological evaluation of M (I)(CO) 3 (NNO) complexes (M= Re, 99mTc) conjugated to 2-(4-aminophenyl) benzothiazole as potential breast cancer radiopharmaceuticals. **Journal of medicinal chemistry**, 49, n. 18, p. 5408-5410, 2006.

TZANOPOULOU, S.; SAGNOU, M.; PARAVATOU-PETSOTAS, M.; GOURNI, E. *et al.* Evaluation of Re and 99mTc complexes of 2-(4′-aminophenyl) benzothiazole as potential breast cancer radiopharmaceuticals. **Journal of medicinal chemistry**, 53, n. 12, p. 4633-4641, 2010.

VAN LENTHE, E.; BAERENDS, E.-J.; SNIJDERS, J. G. Relativistic total energy using regular approximations. **The Journal of chemical physics**, 101, n. 11, p. 9783-9792, 1994.

VAN LENTHE, E.; VAN LEEUWEN, R.; BAERENDS, E. J.; SNIJDERS, J. G. Relativistic regular two-component Hamiltonians. **International Journal of Quantum Chemistry**, 57, n. 3, p. 281-293, 1996.

VAN LENTHE, E. V.; SNIJDERS, J. G.; BAERENDS, E. J. The zero-order regular approximation for relativistic effects: The effect of spin–orbit coupling in closed shell molecules. **The Journal of chemical physics**, 105, n. 15, p. 6505-6516, 1996.

VOLKERT, W. A.; HOFFMAN, T. J. Therapeutic Radiopharmaceuticals. **Chemical Reviews**, 99, n. 9, p. 2269-2292, 1999/09/08 1999.

WAHSNER, J.; GALE, E. M.; RODRÍGUEZ-RODRÍGUEZ, A.; CARAVAN, P. Chemistry of MRI Contrast Agents: Current Challenges and New Frontiers. **Chemical Reviews**, 119, n. 2, p. 957-1057, 2019/01/23 2019.

WAKS, A. G.; WINER, E. P. Breast cancer treatment: a review. **Jama**, 321, n. 3, p. 288-300, 2019.

WRIGHTON, M.; MORSE, D. L. Nature of the lowest excited state in tricarbonylchloro-1,10-phenanthrolinerhenium(I) and related complexes. **Journal of the American Chemical Society**, 96, n. 4, p. 998-1003, 1974/02/01 1974.

YOU, C.; YU, J.; SUN, Y.; LUO, Y. *et al.* Enhanced cytotoxicity by a benzothiazole-containing cisplatin derivative in breast cancer cells. **New Journal of Chemistry**, 41, n. 2, p. 773-785, 2017.

ZHU, X.; ZHANG, F.; KUANG, D.; DENG, G. *et al.* K2S as Sulfur Source and DMSO as Carbon Source for the Synthesis of 2-Unsubstituted Benzothiazoles. **Organic Letters**, 22, n. 10, p. 3789-3793, 2020/05/15 2020.

ZÚÑIGA, C.; OYARZÚN, D. P.; MARTIN-TRANSACO, R.; YÁÑEZ-S, M. *et al.* Synthesis, characterization and relativistic DFT studies of fac-Re (CO) 3 (isonicotinic acid) 2Cl complex. **Chemical Physics Letters**, 688, p. 66-73, 2017.

SECOND PART

ARTICLE 1

Journal: Journal of Chemistry – Submitted for publication

Journal of Chemistry

Exploring EPR Parameters of ^{187}Re Complexes for Designing new MRI Probes: from the gas phase to solution and a model protein environment

Gustavo A. Andolpho[1], Elaine F. F. da Cunha[1*] and Teodorico C. Ramalho[1,2†]

[1]Chemistry Department, Federal University of Lavras, Lavras, Brazil
[2] Center for Basic and Applied Research, Faculty of Informatics and Management, University Hradec Kralove, Hradec Kralove, Czech Republic

Correspondence should be addressed to Teodorico C. Ramalho; †teo@ufla.br or Elaine F.F. da Cunha * elaine_cunha@ufla.br

Abstract

Breast cancer is one of the major types of cancer around the world and early diagnosis is essential to successful treatment. New contrast agents (CA), with reduced toxicology, are needed to improve diagnosis. One of the most promising Magnetic Resonance Imaging (MRI) CA is based on Rhenium conjugated with a benzothiazole derivate (ReABT). In this sense, DFT has been used to evaluate the best methodology for calculating the hyperfine coupling constant (A_{iso}) of ReABT. These results confirm that the relativistic effects and the solvent environment are important for calculating the A_{iso} values. Then, a thermodynamic analysis was performed to confirm the stability of the complex, indicating that Rhenium won't be released from the complex. To understand the interactions between the complex and the target protein, a A_{iso} analysis was performed with the ReABT docked at the enzyme PI3K active site. Our findings point that the Rhenium is strongly bonded in the complex, indicating that the ReABT present lower toxicity, and, the A_{iso} value decreases significantly when the CA candidate ReABT is docked in the active site of the PI3K enzyme, as occurs in the breast cancer cells, showing that this compound could be a good candidate for new contrast agents.

Introduction

Female breast cancer is expected to be the major type of cancer, besides non-melanoma skin tumors, in Brazil between 2020 and 2022, affecting over 66 thousand cases per year according to the National Institute of Cancer José Alencar – INCA [1]. Across the world, data from the American Cancer Society point out that in 2020 over 275,000 cases would be diagnosed in the US and, according to the European Cancer Information System – ECIS, in the European Union over 355,000 cases would be diagnosed in 2020 [2, 3].

Early diagnosis is fundamental to the successful treatment of breast cancer. In this context, many techniques can be applied to help in the diagnosis, like mammography, PET, CT, SPECT, and, MRI [4]. The last one has aroused great interest due to its high sensitivity for the identification and characterization of breast cancer and is successful for early diagnosis [5-7].

This technique is based on the principles of NMR spectroscopy, where the signals came from the relaxation time of hydrogen and oxygen nuclei after the application of a radio frequency [8]. The use of more efficient contrast agents (CA) leads to a better resolution of

the images and can cause an adjustment in the longitudinal and transversal relaxation times, T_1 and T_2 respectively [5, 8, 9]. The hyperfine interactions, which are those related to the interactions between nuclear and electron spins, of paramagnetic species change the relaxation times and can be obtained by EPR spectroscopy [9, 10].

The hyperfine coupling (A) depends on the contributions of isotropic (A_{iso}) and dipolar (A_{dip}) hyperfine coupling constants (Eq. (1)) [9, 10]. The first one comes from unpaired spin in s orbital and the second one results from nonlocal and local dipolar constant. Nevertheless, the dipolar hyperfine coupling constant is close to zero when fluid solutions are considered [9, 10]. These parameters, since it affects the relaxation times and hence present activity in the EPR, is crucial for studying and designing new contrast agents for MRI [9, 10].

$$A = A_{iso} + A_{dip} \quad (1)$$

Traditionally, CAs are metal-based structures like Gd, Pt, and Tc, for example. The study of new CA is important due to the need for increasingly efficient agents, providing better images from the relaxation time of water molecules [11, 12]. Among these metals, we can highlight Tc, highly applied and studied as a contrast agent, and Re, a metal that has great potential as CA due to its low toxicity [5, 13-17].

Re compounds, especially those that have the *fac*-$[Re(CO)_3]^+$ fragment, have been extensively studied as a diagnostic agent for breast cancer. Tzanopoulou et al., 2006, presented this fragment conjugated to the phenylbenzothiazolic derivative, 2-(4-Aminophenyl) benzothiazole (ABT) (Figure 1), as an agent with potential application for MRI [15]. The ABT compound shows great biological activity as anti-bacterial, anti-fungal, anti-allergic, anti-inflammatory, and, in our interest, anti-cancer and inhibiting some enzymes, such as the enzyme kinase [14, 18], especially the phosphoinositide 3-kinase (PI3K) enzyme, which is related with the growth of tumors, like breast cancer [19].

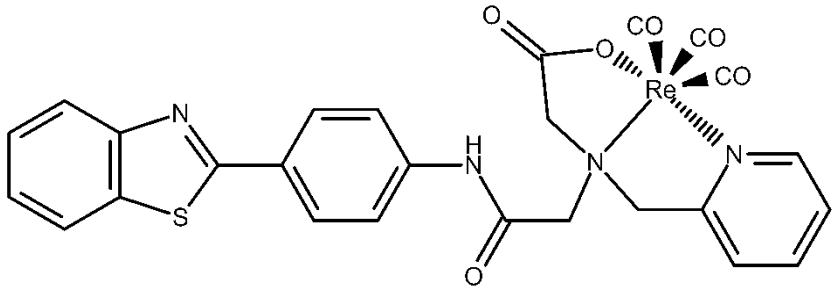

Figure 1. $Re(CO)_3(NNO)$ conjugated with 2-(4'-aminophenyl) benzothiazole.

The compounds of ^{186}Re and ^{188}Re have the potential for medicinal applications, once both can present β emission and have a half-life time equal to 3.8 and 0.7d, respectively [11]. The *fac*-$[Re(CO)_3]$ core presents low-spin, this characteristic, allied with the characteristics previously presented, provides the high interest in this family of compounds for use as radiopharmaceutical [14]. This leads to a broad study of the application of these compounds in EPR spectroscopy and MRI [14] and the need to evaluate the solvent and environment effects on the EPR parameters, which module the action of this compound as a potential MRI contrast agent. Therefore, the objective of this work was to study solvent and relativistic effects on

spectroscopic properties (A_{iso} values for ^{1}H and ^{17}O) of the complex $Re(CO)_3(NNO)$ conjugated with 2-(4'-aminophenyl) benzothiazole.

Materials and Methods

Structural Evaluation

The first step was to perform a geometry optimization calculation for the $Re(CO)_3(NNO)$ conjugated to 2-(4'-aminophenyl) benzothiazole, ReABT. This calculation was performed using the DFT method, using the ωB97X-D3 hybrid-GGA functional [20], using TZVP basis set for all atoms except Re and SARC-ZORA-TZVP [21] for Rhenium, and considering the Zero Order Regular Approximation – ZORA [22] on software ORCA 4.2.1 [23].

Spectroscopic Calculations

For the hyperfine coupling constant calculations (A_{iso}), the Density Functional Theory was also used, taking the geometry of minimum energy obtained, applying different approaches to define which methodology works better in our compound. To do that, three different functionals were used, the GGA functional of Perdew-Burke-Ernzerhof, PBE [24], the hybrid-GGA functional PBE0, which mixes the PBE exchange energy with the Hartree-Fock exchange energy [25], and the meta-hybrid GGA functional Minessota 06-L, M06-L [26].

The solvent effect was also analyzed by theoretical calculations carried out in the vacuum and the presence of water as solvent [27]. The solvation method used was the Conductor-like Polarizable Continuum Model, CPCM, since it considers the solvent as a polarizable conductor, so it can describe molecules that interact with polar solvents, like water [28].

So, in the first step, the solvent effect was analyzed. In the second step, relativistic effects were evaluated, to this end, calculations considering these effects in the Hamiltonian with ZORA, using the SARC-ZORA-TZVP basis set for Rhenium atom and TZVP for all other atoms, and non-relativistic calculations were performed with the def2-TZVP basis set for Rhenium and TZVP for all other atoms was used to perform calculations. These three steps will provide us with a methodology that fits better with the compound under study.

Thermodynamics investigation and molecular docking calculation

To understand if the complex is thermodynamically stable, a frequency calculation, using M06L functional, SARC-ZORA-TZVP basis set for Rhenium and TZVP for all other atoms and relativistic effects in the Hamiltonian with ZORA, was performed in the ReABT complex, in the $Re(CO)_3^+$ core (Figure 2.c), and in the tridentate ligand, (NNO)ABT (Figure 2.b). This analysis will provide the free energy of complexation of the complex (Fig. 2.a and Eq. (2)), allowing us to understand if the Rhenium core is strongly bonded in the complex [29].

$$\Delta G_{Aq} = \Delta G_{SOLV}(ReABT) - [\Delta G_{SOLV}(Re(CO)_3) + \Delta G_{SOLV}((NNO)ABT)] + \Delta G_g \quad (2)$$

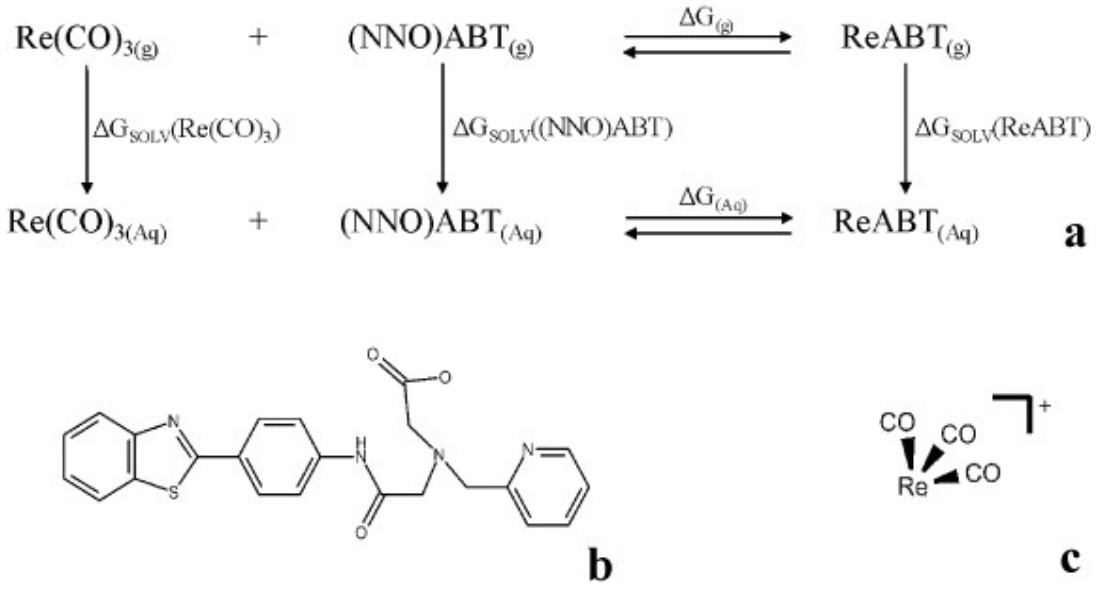

Figure 2. (a) Thermodynamic cycle. (b) (NNO)ABT. (c) $Re(CO)_3^+$.

The molecular docking of the complex in the PI3K enzyme active site was performed to obtain A_{iso} values for the compound [7, 17]. For this, the complex was docked inside of the PI3K enzyme (Protein Data Bank (PDB) code 3QJZ [30]) using the software Molegro Virtual Docking (MVD) [31]. The conformation that most closely matches the active ligand of the PI3K enzyme, with the amino acids residues that perform hydrogen bonds (H-Bonds) in the PI3K active site, was selected to calculate Hyperfine Coupling Constant values using the methodology defined previously.

Results and Discussion

The results provided in this paper were divided into four major parts, the first one is the structural results, which provide the geometry of minimum energy for the complex $Re(CO)_3$(NNO) conjugated with 2-(4'-aminophenyl) benzothiazole (ReABT). The second step is to determine the best theoretical methodology to calculate A_{iso} values of ReABT, where we discussed the solvent and relativistic effects. The next section will discuss the thermodynamics of the complex, to evaluate the free energy of complexation. In the last part of the results, the methodology defined previously was applied to analyze how A_{iso} values of the ReABT complex change when the complex was docked in the PI3K active site.

Structural Investigation

The geometry optimization of complex ReABT was performed using DFT calculation with the functional ωB97X-D3, considering relativistic effects by using ZORA, with TZVP basis set for H, C, O, N, and S atoms and SARC-ZORA-TZVP basis set for Re. The optimized geometry was presented in Figure 3, with the main bond lengths highlighted. These bond lengths were presented in Table 1, once are no crystallographic data from ReABT, we use experimental results obtained by Machura et al., 2011, for the complex $Re(CO)_3Cl$ conjugated to 2-(2-aminophenyl) benzothiazole (ReAPBT) [13].

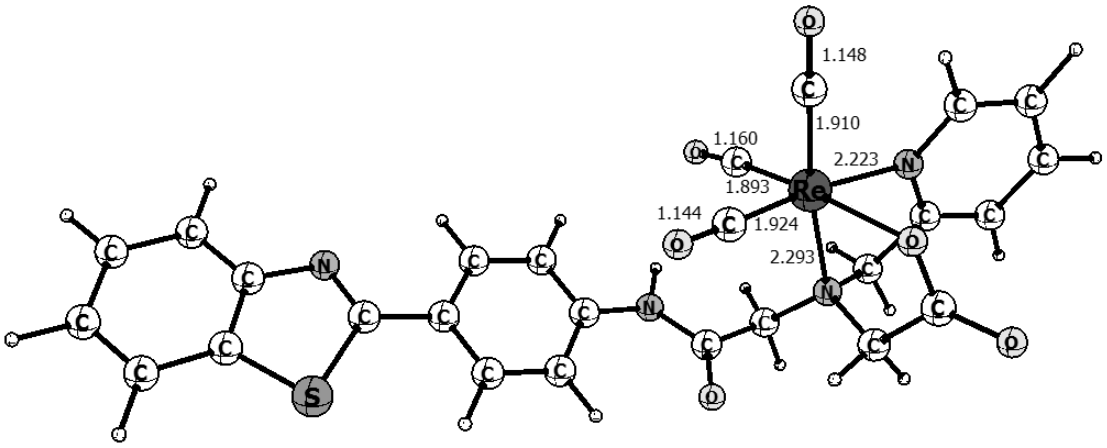

Figure 3. $Re(CO)_3(NNO)$ conjugated to 2-(4'-aminophenyl) benzothiazole optimized structure, with some bond lengths highlighted, in Angstrom.

Table 1. Lengths of some bonds of the ReABT (Theoretical) and ReAPBT (Experimental) complexes.

Bond lengths	Length (Å)	
	Theoretical	Experimental
$Re - C_{ax}$	1.910	1.897
$Re - C_{eq1}$	1.924	1.901
$Re - C_{eq2}$	1.893	1.908
$Re - N_{ax}$	2.293	2.179
$Re - N_{eq}$	2.223	2.244
$C_{ax} - O$	1.148	1.157
$C_{eq1} - O$	1.160	1.155
$C_{eq2} - O$	1.144	1.151

To confirm if the theoretical values for the bonds of our complex, Table 1, are in agreement with experimental data, structural parameters from our theoretical findings were compared to Machura´s work [13]. It should be kept in mind, however, that the equatorial bond between Re-O in our complex does not exist in the compound studied by Machura and co-workers [13], so this change can affect the other bonds. The main difference is in the $Re-N_{ax}$ bond, with 0.114 Å longer in the theoretical result. The C-O bonds are shorter ranging from 0.005 and 0.009 Å. Differences from the bond lengths have a medium value of 0.026 Å.

To improve the structural analysis, we compared the bond angles among theoretical and experimental values obtained from the work of Machura and co-workers (Table 2). The differences in bond angles, presented in Table 2, range from 0.25°, for the $C_{eq} - Re - C_{eq}$ bond, and 5.07° for the $C_{eq1} - Re - C_{eq2}$ bond when compared with experimental data of Machura and co-workers paper [13]. These results of bond lengths and bond angles show that our result of geometry optimization is in agreement with experimental results.

Table 2. Dihedral angles of some connections of the ReABT (Theoretical) and ReAPBT (Experimental).

Bond Angle	Angle (°)	
	Theoretical	Experimental
$Re - C - O_{ax}$	178.84	175.8
$Re - C - O_{eq1}$	174.45	176.5
$Re - C - O_{eq2}$	177.21	179.9
$N_{eq} - Re - N_{ax}$	76.70	77.15

C_{eq} – Re - C_{eq}	89.03	88.78
C_{eq2} – Re - C_{ax}	86.51	87.9
C_{eq1} – Re - C_{ax}	89.57	84.5

Solvent and Relativistic Effects on Hyperfine Coupling Constant Calculations

Once the geometry of the complex was optimized, hyperfine coupling constant calculations, A_{iso}, were carried out. First, the solvent effect has been evaluated on the A_{iso} values. For that, theoretical calculations considering ReABT in the gas phase and solution with relativistic effects were performed [32]. Our theoretical findings are presented in Table 3.

Table 3. Hyperfine coupling constants, Aiso, in MHz, for three different functionals, in the gas phase and solution, using relativistic effect (SARC-ZORA-TZVP for Re, TZVP for all other atoms, and ZORA in the Hamiltonian).

Functional		^{1}H	^{17}O	^{187}Re
M06L	Gas Phase	2.937	2.528	96.658
	Solution	2.656	1.445	36.311
PBE	Gas Phase	1.694	1.171	51.851
	Solution	1.588	0.629	24.903
PBE0	Gas Phase	1.956	0.669	9.560
	Solution	1.947	0.586	9.195
Exp [32]	—	—	—	*38.000*

As seen in Table 3, the differences among A_{iso} results in solution are small. The larger differences are between the gas phase and solution, for oxygen, about 1.084 MHz, using M06L functional, 0.543 MHz, for the PBE functional, and 0.083 MHz, when the functional used is PBE0. For hydrogen atoms, these differences are 0.281, 0.106, and 0.009 MHz, for M06L, PBE, and PBE0 functionals, respectively. This result shows that the complex in water, as occurs in the biological environment and human body, can decrease the hyperfine coupling constant values when compared to the result in the gas phase.

A large difference between A_{iso} results of Re can be observed, except for the PBE0 functional, where the difference is about 0.365 MHz, being smaller in the solvent. For the functionals PBE and M06L, the decrease was approximated 26.948 and 60.347 MHz, respectively, when the solvation model was applied.

In spite of its great importance, to our knowledge, this is the first investigation of $^{185|187}Re$ hyperfine coupling constant values for the ReABT complex. To compare our result, we use the result obtained by Lunsford et al., 2017, which points to the A_{iso} value for $^{185|187}Re$ in a $Re(CO)_3$ core as 38 MHz [33]. Thus, our findings point out that calculation using the Minessota 06-L functional in solution agrees with the result obtained in the literature.

Once the computational cost for applying the relativistic effects in the Hamiltonian and the basis set are large, we perform a non-relativistic calculation. Since the previous results show that the solvent effect was important, all calculations were performed including the solvent effect.

Then, since the computational cost for introducing relativistic effects is higher, we have investigated the impact of the relativistic effects on the Aiso values of the spectroscopic probe ReABT (Figure 1). These results are presented in Table 4 and, as expected, show poor results for non-relativistic calculations of $^{185|187}$Re hyperfine coupling constant values. So, our findings put in evidence that the relativistic effects are needed for calculating more accurate Aiso values of ReABT.

Table 4. Hyperfine coupling constants, A_{iso}, in MHz, for three different functionals, in solution, and without relativistic effect.

Functional	^{1}H	^{17}O	^{187}Re
M06L	3.433	15.789	0.006
PBE	2.068	2.558	0.017
PBE0	3.127	6.051	0.016
Exp [32]	—	—	*38.000*

The results presented in Table 4 pointed that, as expected, the Aiso value decrease drastically for Rhenium, being 9.179, 24.886, and 36.305 MHz smaller for PBE0, PBE, and M06L functionals, respectively, when the relativistic effect was not included in the calculations. For the oxygen and hydrogen atoms, the Aiso value increased when the relativistic effect was not present. For hydrogen, the increase was 1.180, 0.480, and 0.777 MHz for PBE0, PBE, and M06L functionals, respectively, as for oxygen, the increase was 5.465, 1.929, and 14.344 MHz for PBE0, PBE, and M06L functionals, respectively.

From these A_{iso} theoretical findings, it is possible to define the best theoretical strategy, combination of functional, solvent model, and relativistic effect. For the spectroscopic probe ReABT, the best combination is using the M06L functional considering relativistic effects on Zeroth Order Regular Approximation, with the SARC-ZORA-TZVP basis set for Re and solvent effects evaluated at the CPCM level.

Thermodynamics evaluation for the complex stability: toxicologic properties

Currently, most Contrast Agents (CAs) used for MRI are Gd-based compounds. They perform well for the improved images provided by MR. However, in the early 2000s, a life-threatening disease, the Nephrogenic Systemic Fibrosis, was associated with these CAs, once they release free Gd ions. Since then, the search for new CAs with low toxicity and high performance has intensified [34, 35].

Rhenium-based CAs, like the ReABT, were studied due to their potential as spectroscopy probes and low toxicity [15]. A study by Breitz *et al.* shows that compounds with Rhenium atoms, despite showing accumulation in the kidneys, do not present an influence on renal activity [36]. To understand if the complex in the study does not release free Re ions, the free energy of complexation, according to the thermodynamic cycle presented in Figure 2, has been calculated.

The result obtained for the Gibbs free energy of complexation, -744.37 kcal/mol, at the M06-L level, with the Zeroth Order Regular Approximation – ZORA and SARC-ZORA-TZVP basis set for Rhenium and TZVP for all other atoms, is strongly negative and indicates that the complex is stable in solution. In this way, the complex ReABT shows low toxicity due to its high stability, which will theoretically not show the dissociation of Re ions. Now that our findings have pointed out that the complex shows high stability in solution, it is possible to move on to the next step of this paper, where the hyperfine coupling constant values for ReABT when docked at the active site of the enzyme will be evaluated.

Molecular Interaction between ReABT and the target protein: Docking Studies

The early diagnosis is crucial for the successful treatment of any disease, especially for breast cancer [4]. For that, the use of spectroscopic probes able to interact with specific molecular targets is important. In breast cancer, this molecular target is the enzyme phosphoinositide 3-kinase (PI3K), which is closely linked to the growth of cancer cells in this tissue [19]. The compounds of the benzothiazole family are known inhibitors of the enzyme kinase family, especially, the PI3K enzyme [7, 17, 37, 38]. In this context, the study of the interaction between the complex ReABT and the enzyme PI3K is important and was investigated in our work using docking calculations.

First, it is possible to check the position of the compound in the active site by taking the overlap and orientation according to the active ligand, N-{6-[(2-(methylsulfanyl)pyrimidin-4yl]- 1, 3-benzothiazol-2-yl} acetamide, a benzothiazole derived (Figure 4).

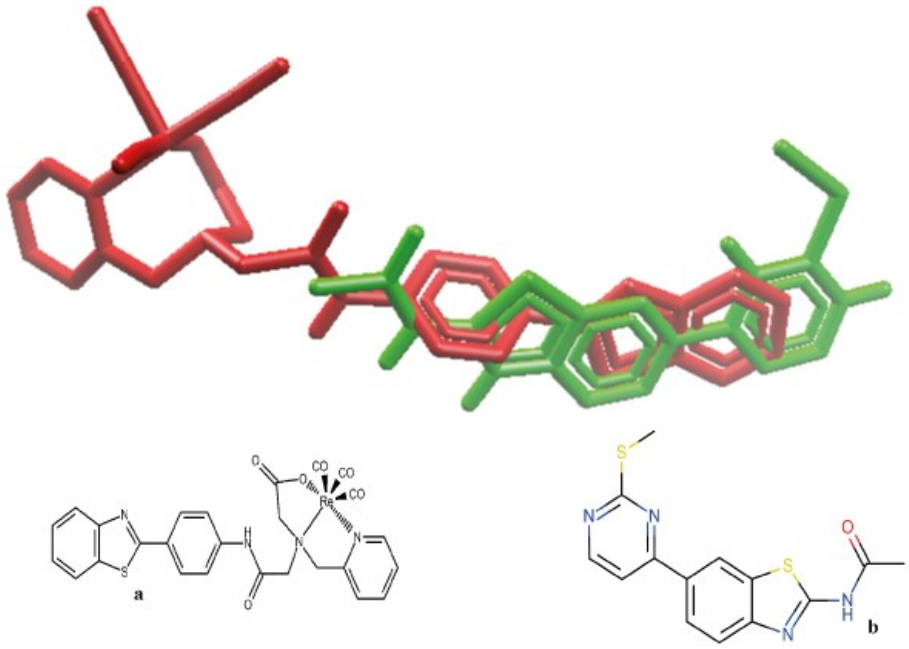

Figure 4. ReABT in red (structure in part a) and active ligand in green (structure in part b) docked in the PI3K (PDB code 3QJZ) active site.

To continue the analysis of the docking calculation, we can investigate the hydrogen bonds that the ReABT performs inside the active site. In Figure 5, it is possible to observe that ReABT

interacts, by means of H-bonds, with amino acids residues Val882, Lys883, and Asp884. It is important to highlight that the active ligand of the PI3K enzyme interacts with the amino acid residue Val882. The intermolecular interaction energy of the active ligand was equal to -121.17 kcal mol^{-1} and -163.62 kcal mol^{-1} for the ReABT. These results pointed out that the complex ReABT could have better stability in the active site of the PI3K enzyme. Meanwhile, it must be highlighted that these results do not consider pharmacokinetic properties.

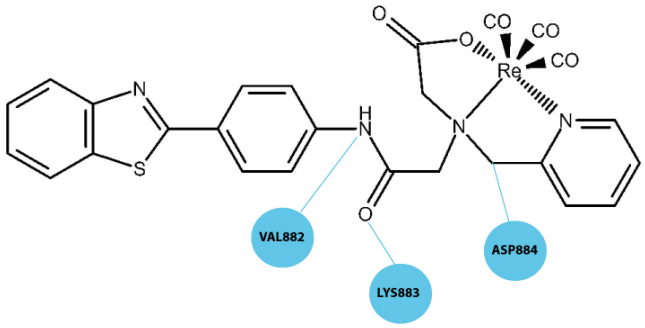

Figure 5. H-Bonds performed in molecular docking simulation with the ReABT-PI3K system.

Now, the theoretical methodology defined in the hyperfine coupling constant study has been applied for analyzing the change of the Aiso value when the ReABT complex is in the active site of the PI3K enzyme. The calculation was performed using the DTF, with M06L functional, ZORA in the Hamiltonian, SARC-ZORA-TZVP basis set for Re, and TZVP for all other atoms. This calculation shows that the A_{iso} value for ^{187}Re decreased from 36.311 MHz to 0.0571 MHZ, while for ^{1}H the decrease was from 2.656 MHz to 0.0236 MHz and from 1.445 MHz to 0.0018 MHz for ^{17}O. This dramatic change indicates that the ReABT shows activity on EPR in the active site of PI3K, showing its potential for the development of a new spectroscopic probe.

Conclusions

From our data, the best calculation level for obtaining the hyperfine coupling constant (A_{iso}) for the complex $Re(CO)_3(NNO)$ conjugated to 2-(4'-aminophenyl) benzothiazole is with the M06L functional, SARC-ZORA-TZVP basis set for Re and TZVP for all other atoms, considering the relativistic effects in the Hamiltonian with ZORA and using implicit solvation method CPCM. The thermodynamic analysis shows us that the ReABT complex is stable and should not release free Rhenium on biologic systems. In this sense, the toxicologic risks associated with the complex are considerably reduced.

The best theoretical strategy has been selected and applied to ReABT. This complex was docked in the PI3K active site and it was possible to observe a huge decrease for the A_{iso} values for ^{1}H, ^{17}O, and ^{187}Re, showing activity on EPR. This finding reveals that the complex $Re(CO)_3(NNO)$ conjugates to 2-(4'-aminophenyl) benzothiazole has the potential to lead the development of a new spectroscopic probe for diagnosis cases of breast cancer.

Conflicts of Interest

The authors declares that there is no conflict of interest regarding the publication of this paper.

Funding Statement

This work was supported by Brazilian financial agencies Conselho Nacional de Desenvolvimento Científico e Tecnológio, Fundação de Amparo ao Ensino e Pesquisa de Minas Gerais and Coordenação de Aperfeiçoamento de Pessoal de Nível Superior for financial support, and the Federal University of Lavras for providing the physical infrastructure and work space.

References

[1] INCA, Instituto Nacional de Câncer José Alencar Gomes da Silva. [Estimated 2018: Cancer Incidence in Brazil.] Rio de Janeiro. INCA RJ: 2019. Portuguse.

[2] American Cancer Society. Breast Cancer Facts & Figures 2019-2020. American Cancer Society, Inc: Atlanta, 2019.

[3] European Cancer Information System. Breast cancer burden in EU-27. European Union, 2020.

[4] Jafari SH, Saadatpour Z, Salmaninejad A, et al. Breast cancer diagnosis: Imaging techniques and biochemical markers. J. Cell. Physiol. **2018,** *233* (7), 5200-5213.

[5] Pereira BTL, Silva ÉF, Gonçalves MA, et al. Exploring EPR Parameters of ^{99}Tc Complexes for Designing New MRI Probes: Coordination Environment, Solvent, and Thermal Effects on the Spectroscopic Properties. J. Chem. **2017,** *2017*, 8102812.

[6] Hu Q, Whitney HM, Giger ML. A deep learning methodology for improved breast cancer diagnosis using multiparametric MRI. Sci. Rep. **2020,** *10* (1), 1-11.

[7] Corrêa S, Rosa IA, Andolpho GA, et al. Hybrid Materials Based on Magnetic Iron Oxides with Benzothiazole Derivatives: A Plausible Potential Spectroscopy Probe. Int. J. Mol. Sci. **2021,** *22* (8).

[8] Long N, Wong W. The chemistry of molecular imaging. New Jersey: John Wiley & Sons; 2014.

[9] Gonçalves MA, da Cunha EFF, Peixoto FC, et al. Probing thermal and solvent effects on hyperfine interactions and spin relaxation rate of δ-FeOOH(100) and [MnH3buea(OH)]2−: Toward new MRI probes. Comput. Theor. Chem. **2015,** *1069*, 96-104.

[10] Look DC, Locker DR. Time Saving in Measurement of NMR and EPR Relaxation Times. Rev. Sci. Instrum. **1970,** *41* (2), 250-251.

[11] Wahsner J, Gale EM, Rodríguez-Rodríguez A, et al. Chemistry of MRI Contrast Agents: Current Challenges and New Frontiers. Chem. Rev. **2019,** *119* (2), 957-1057.

[12] Gonçalves MA, Santos LS, Peixoto FC, et al. Comparing Structure and Dynamics of Solvation of Different Iron Oxide Phases for Enhanced Magnetic Resonance Imaging. ChemistrySelect. **2017,** *2* (31), 10136-10142.

[13] Machura B, Wolff M, Gryca I, et al. Novel Re(I) tricarbonyl complexes of chelating ligands with aromatic N-heterocycle ring and aliphatic amine donor – Synthesis, spectroscopic characterization, X-ray structure and DFT calculations. Polyhedron. **2011,** *30* (13), 2275-2285.

[14] Machura B, Wolff M, Benoist E, et al. Tricarbonyl rhenium(I) complex of benzothiazole – Synthesis, spectroscopic characterization, X-ray crystal structure and DFT calculations. J. Organomet. Chem. **2013,** *724*, 82-87.

[15] Tzanopoulou S, Pirmettis IC, Patsis G, et al. Synthesis, characterization, and biological evaluation of M (I)(CO) 3 (NNO) complexes (M= Re, 99mTc) conjugated to 2-(4-aminophenyl) benzothiazole as potential breast cancer radiopharmaceuticals. J. Med. Chem. **2006,** *49* (18), 5408-5410.

[16] Tzanopoulou S, Sagnou M, Paravatou-Petsotas M, et al. Evaluation of Re and 99mTc complexes of 2-(4′-aminophenyl) benzothiazole as potential breast cancer radiopharmaceuticals. J. Med. Chem. **2010,** *53* (12), 4633-4641.

[17] Mancini DT, Souza EF, Caetano MS, et al. ^{99}Tc NMR as a promising technique for structural investigation of biomolecules: theoretical studies on the solvent and thermal effects of phenylbenzothiazole complex. Mag. Reson. Chem. **2014,** *52* (4), 129-137.

[18] Mavroidi B, Sagnou M, Stamatakis K, et al. Palladium (II) and platinum (II) complexes of derivatives of 2-(4′-aminophenyl) benzothiazole as potential anticancer agents. Inorganica Chim. Acta. **2016,** *444*, 63-75.

[19] Janku F. Phosphoinositide 3-kinase (PI3K) pathway inhibitors in solid tumors: From laboratory to patients. Cancer Treatment Reviews, **2017**, 59, p. 93-101.

[20] Lin YS, Li GD, Mao SP, et al. Long-Range Corrected Hybrid Density Functionals with Improved Dispersion Corrections. J. Chem. Theory Comput. **2013,** *9* (1), 263-272.

[21] Pantazis DA, Chen XY, Landis CR, et al. All-electron scalar relativistic basis sets for third-row transition metal atoms. J. Chem. Theory Comput. **2008,** *4* (6), 908-919.

[22] van Wüllen C. Molecular density functional calculations in the regular relativistic approximation: Method, application to coinage metal diatomics, hydrides, fluorides and chlorides, and comparison with first-order relativistic calculations. J. Chem. Phys. **1998,** *109* (2), 392-399.

[23] Neese F. Software update: the ORCA program system, version 4.0. Wiley Interdiscip. Rev.: Comput. Mol. Sci. **2018,** *8* (1), e1327.

[24] Perdew JP, Burke K, Ernzerhof M. Generalized gradient approximation made simple. Phys. Re. Lett. **1996,** *77* (18), 3865.

[25] Adamo C, Barone V. Toward reliable density functional methods without adjustable parameters: The PBE0 model. J. Chem. Phys. **1999,** *110* (13), 6158-6170.

[26] Zhao Y, Truhlar DG. A new local density functional for main-group thermochemistry, transition metal bonding, thermochemical kinetics, and noncovalent interactions. J. Chem. Phys. **2006,** *125* (19), 194101.

[27] Toledo EJL, Ramalho TC. Controversies about hydrogen bonds in water molecules on the influence of high magnetic fields: implications on structural and electronic parameters. Mol. Simul. **2021,** *47* (14), 1159-1167.

[28] Cossi M, Rega N, Scalmani G, et al. Energies, structures, and electronic properties of molecules in solution with the C-PCM solvation model. J. Comput. Chem. **2003,** *24* (6), 669-681.

[29] Braga LS, Silva ÉF, Mancini DT, et al. Detection of Chemical Weapon Agents Using Spectroscopic Probes: A Computational Study. J. Chem. **2020,** *2020*, 1312403.

[30] D'Angelo ND, Kim TS, Andrews K, et al. Discovery and optimization of a series of benzothiazole phosphoinositide 3-kinase (PI3K)/mammalian target of rapamycin (mTOR) dual inhibitors. J. Med. Chem. **2011,** *54* (6), 1789-1811.

[31] Thomsen R, Christensen MH. MolDock: a new technique for high-accuracy molecular docking. J. Med. Chem. **2006,** *49* (11), 3315-3321.

[32] Pyykkö P. Relativistic effects in chemistry: more common than you thought. Annu. Rev. Phys. Chem. **2012,** *63*, 45-64.

[33] Lunsford AM, Goldstein KF, Cohan MA, et al. Comparisons of MN 2 S 2 vs. bipyridine as redox-active ligands to manganese and rhenium in (L–L) M′(CO) 3 Cl complexes. Dalton Trans. **2017,** *46* (16), 5175-5182.

[34] Hasebroock KM, Serkova NJ. Toxicity of MRI and CT contrast agents. Expert. Opin. Drug Metab. Toxicol. **2009,** *5* (4), 403-416.

[35] Chehabeddine L, Al Saleh T, Baalbaki M, et al. Cumulative administrations of gadolinium-based contrast agents: risks of accumulation and toxicity of linear vs macrocyclic agents. Crit. Rev. Toxicol. **2019,** *49* (3), 262-279.

[36] Breitz HB, Durham JS, Fisher DR, et al. Pharmacokinetics and normal organ dosimetry following intraperitoneal rhenium-186-labeled monoclonal antibody. J. Nucl. Med. **1995,** *36* (5), 754-761.

[37] Pereira AF, Prandi IG, Ramalho TC. Parameterization and validation of a new force field for Pt (II) complexes of 2-(4′-amino-2′-hydroxyphenyl) benzothiazole. International Journal of Quantum Chemistry, **2021**, 121(6):e26525.

[38] da Cunha EF, Sippl W, Ramalho TC, et al. 3D-QSAR CoMFA/CoMSIA models based on theoretical active conformers of HOE/BAY-793 analogs derived from HIV-1 protease inhibitor complexes. European journal of medicinal chemistry, **2009**, 44(11):4344-52.

ARTICLE 2

Journal: Journal of Molecular Modeling – Submitted for publication

Insights into the value of statistical models, solvent and relativistic effects for investigating Re complexes of benzothiazole derivatives: potential spectroscopic probes

Gustavo A. Andolpho[1], Elaine F. F. da Cunha[1], and Teodorico C. Ramalho[1,2].*

[1] Chemistry Department, Federal University of Lavras, P.O. Box 3037, 37200-900 Lavras, MG, Brazil.

[2] Center for Basic and Applied Research, Faculty of Informatics and Management, University of Hradec Kralove, Hradec Kralove, Czech Republic.

Corresponding author: Teodorico C. Ramalho

e-mail: teo@ufla.br

Tel.: +55 35 3829-1522

ACKNOWLEDGMENT

We are grateful for the support of Conselho Nacional de Desenvolvimento Científico e Tecnológico (CNPq), Fundação de Amparo à Pesquisa do Estado de Minas Gerais (FAPEMIG) and Coordenação de Aperfeiçoamento de Pessoal de Nível Superior – Brasil (CAPES).

ABSTRACT

Cancer affects a major part of the worldwide population and, to minimize deaths, the diagnosis in the early stages of the disease is fundamental. Thus, to improve diagnosis and treatment new potential spectroscopic probes are crucial. Benzothiazole derivates present antitumor properties and are highly selective and interact strongly with the protein Phosphoinositide 3-kinase (PI3K), which was associated with cell proliferation and breast cancer cells. In this paper, the Rhenium shielding tensors (^{187}Re(σ)) and hydrogen and carbon chemical shifts (^{1}H(δ) and ^{13}C(δ)) of the $Re(CO)_3$(NNO) complex conjugated with 2-(4'-aminophenyl)benzothiazole (ReABT) were evaluated. A statistical HCA model was used to analyze the best DFT protocol to compute σ and δ values and to evaluate the relativistic effects, both in the basis set and Hamiltonian as well as the functionals M06L or PBE0. The best protocol was applied to obtain ^{187}Re(σ) of the ReABT complex in different environments (gas phase, solution, and in the active site of the PI3K enzyme). The results point out that ^{187}Re(σ) values of the ReABT complex change significantly when the complex is docked in the PI3K enzyme.

KEYWORDS: $ReCO_3$, DFT, RMN, HCA

1. INTRODUCTION

Cancer affects a major part of the worldwide population. It was estimated that more than 19 million new cases and 10 million deaths would occur in 2020 [1]. Among all these cases, more than 11% and almost 7% of all deaths are related to female breast cancer [1]. In 2019, in the United States, more than 271 thousand cases and more than 42 thousand deaths would be estimated to be related to breast cancer in both sexes [2].

Several studies indicate that to minimize deaths among breast cancer, the diagnosis in the early stages of the disease is fundamental [1, 3-11]. Mammography is the most common diagnosis method, however, some limitations, such as low sensitivity and selectivity, prevent this technique from being successful in a large percentage of diagnoses [3, 5].

Other techniques, such as ultrasonography, positron-emission tomography (PET), single-photon emission computed tomography (SPECT), computed tomography (CT), and magnetic resonance imaging (MRI), can help to improve diagnoses, nonetheless, several problems, mainly related to costs and image quality, hinder the use of these techniques [3, 5]. To improve diagnosis and treatment, the search for new compounds that can act as a contrast agent for spectroscopic techniques, such as MRI, is a great challenge [12, 13].

A candidate was proposed in 2006 by Tzanopoulou and co-workers. They used CAs based on Technetium and Rhenium atoms, the M(CO)3(NNO) conjugated to 2-(4'-Aminophenyl) benzothiazole [14]. In fact, metallic complexes with Tc-based have already been studied in our group and show potential as spectroscopic probes, now we propose to study the Rhenium-based complex [10, 15]. Re-based compounds show promising potential as spectroscopy probes [14, 16-18] and have not presented any influence on renal activity [19].

Benzothiazole derivatives, especially the derivative 2-(4-aminophenyl) Benzothiazole (ABT), has aroused interest for application as CAs since they present antitumor properties and are highly selective, interacting strongly with the protein Phosphoinositide 3-kinase (PI3K), which was associated with several cellular activities, including cell proliferation and breast cancer cells [15, 18, 20].

The complex Re(CO)3(NNO) conjugated to 2-(4'-Aminophenyl) benzothiazole, the ReABT complex (Figure 1), proposed by Tzanopoulou and co-workers, has an affinity for breast tumors since the benzothiazole derivate presents inhibitory activity against breast tumor cells [14]. In this sense, ReABT is a potential new target-

specific breast cancer spectroscopic probe, however, despite its great importance, surprisingly few detailed spectroscopic studies and computational work on Re complexes have appeared [16-18].

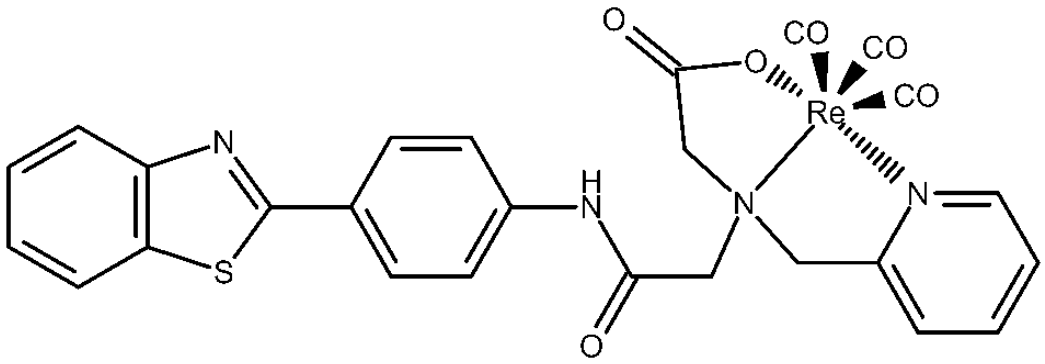

Figure 1. Chemical structure of ReABT.

The NMR study is important for candidates to CAs since the characterization of these compounds makes it possible to better understand their spectroscopic behavior in solution or enzymatic environments [15, 21, 22]. Once the development of new CAs, and pharmaceutical compounds in general, demands a high investment and a long time, the use of computational chemistry techniques is important for the drug development process [15, 23, 24].

Among several theoretical calculation techniques, the density functional theory (DFT) is a useful method that can evaluate many chemical characteristics, including chemical shifts and coupling constants, and can also be used in larger molecules and biological systems [15, 25-28]. This method is also very useful for calculating the properties of atoms and relativistic effects.

Rhenium is an atom of the sixth row of the periodic table, which makes the relativistic effects in Re-based compounds of high importance [29]. So, the use of DFT is interesting for calculating structural and electronic parameters of the ReABT complex.

Therefore, the goal of this work is to study NMR properties of ReABT (Figure 1) to select the best calculation protocol using different DFT functionals, basis sets and relativistic effects. In addition, additional calculations were carried out to evaluate the influence of the solvent effects and enzymatic environment on the NMR spectroscopic properties of ReABT.

2. Materials and Methods

The optimized geometries for the studied complex have been got with the ωB97X-D3 functional [30], the SARC-ZORA-TZVP basis set for Rhenium, and the TZVP basis set for all other atoms [31]. We also used the Zeroth Order Regular Approximation (ZORA) in the Hamiltonian [32].

After the optimization, a factorial 2K model calculation was performed using the Chemoface software [33], to evaluate the influence of basis set, DFT functional, and relativistic effects on spectroscopic parameters [34]. The NMR properties were computed at the GIAO-DFT method [35, 36]. The levels and parameters of the factorial model were presented in Table 1.

The first parameter was the basis set used, being used a non-relativistic one (TZVP) and the basis set with ZORA (ZORA-TZVP). To analyze the influence of relativistic effects on basis sets for the rhenium atom, the basis sets def2-TZVP and SARC-ZORA-TZVP were used as level -1 and +1, respectively. The second parameter explored was the DFT functional, M06L [37], and PBE0 [38] functionals were evaluated in the NMR calculations [39-42]. The last parameter evaluated was the relativistic effect on the Hamiltonian system, non-relativistic Hamiltonian and ZORA Hamiltonian were used as level -1 and +1, respectively. This approach leads us to eight different calculations, involving the three parameters and two levels, which are shown in Table 2.

Table 1. Levels and parameters for the 2^3 factorial model.

Parameter	Level	
	-1	+1
(A) Basis Set	TZVP	ZORA-TZVP
(B) Functional	PBE0	M06L
(C) Relativistic Hamiltonian	Non-relativistic	ZORA

To analyze the 1H and 13C chemical shift values, TMS has been used as a reference. In this case, TMS was optimized and simulated at the same calculation level. All the calculations were performed in the gas phase using the ORCA 5.0.0 software [43]. To evaluate the best calculation protocol, a Hierarchical Cluster Analysis, HCA, was performed on the Chemoface software, which was analyzed, along with reference values, considering the nearest neighbor obtained from the Euclidean distance.

Table 2. 2^3 factorial model, with the levels for the eight cases.

Cases	Level for each parameter		
	A	B	C
1	-1	-1	-1

2	-1	-1	+1
3	-1	+1	-1
4	-1	+1	+1
5	+1	-1	-1
6	+1	-1	+1
7	+1	+1	-1
8	+1	+1	+1

Once the calculation protocol was defined, the solvent effect has been evaluated on chemical shifts values, using water with the CPCM method. Then, an NMR calculation was performed on the ReABT complex docked in the active site of the target enzyme, considering the residues that interact with hydrogen bonds. The docking study was performed with Molegro Virtual Docking software [44], using the PI3K enzyme (Protein Data Bank (PDB) code 3QJZ [45]), adopting the procedure defined by Mancini et al., 2014 and Corrêa et al., 2021 [11, 15].

3. Results and Discussion

3.1. Experimental designing for selecting the best calculation protocol for NMR parameters

The GIAO-DFT method was used for the NMR calculation of all eight cases reported in Table 2. As expected, δ(1H) and δ(13C) results, which are presented in Tables S1 and S2, are close to experimental values when the relativistic effects were included [14].

The differences in the chemical shifts are larger when the relativistic implementation is evaluated with the TZVP basis set. For the non-relativistic basis sets, the perceptual error between our results and the reference value ranges from 27.60 to 398.41%, when the ZORA implementation was used, this error ranges from 6.20 to 23.95%.

In the B parameter, DFT functional, the average error increases when we move from the hybrid functional, PBE0, to the meta-hybrid GGA, M06L, going from 36.74% to 68.24% and from 41.54 to 125.00% for the δ(13C) and δ(1H), respectively.

When the relativistic effects are analyzed in both the Hamiltonian and Basis Set, i.e., cases 6 and 8 in Table 3, against cases 1 and 3, i.e., non-relativistic calculations, the average error decreased significantly. These average errors range from 65.08%, for δ(13C), and 44.27% for δ(1H), for non-relativistic calculations, to 8.27 and

18.09%, for δ(13C) and δ(1H), respectively, when relativistic effects are considered on basis set and Hamiltonian. All the errors are presented in Table 3.

Table 3. Average perceptual errors, relative to experimental values, for the eight cases used for the ^{1}H and ^{13}C chemical shifts calculations.

Cases	1	2	3	4	5	6	7	8
Error (%) δ(^{1}H)	33.36	104.94	55.19	398.41	14.13	13.74	23.95	22.44
Error (%) δ(^{13}C)	27.60	106.65	102.56	153.52	6.51	6.20	10.68	10.34

To confirm the best calculation protocol, a HCA was performed. To do that, all the δ values for 26 carbon atoms and 19 hydrogen atoms (Tables S1 and S2) were considered. The dendrogram explicitly shows that protocol 6, using the ZORA-TZVP basis set, PBE0 functional, and ZORA implementation on the system Hamiltonian is the best calculation protocol. It is important to highlight that although the difference between protocols 5 and 6 is not so large, the computational cost between the two theoretical approaches is not large and the use of relativistic effects in the Hamiltonian is important for σ(187Re) calculations.

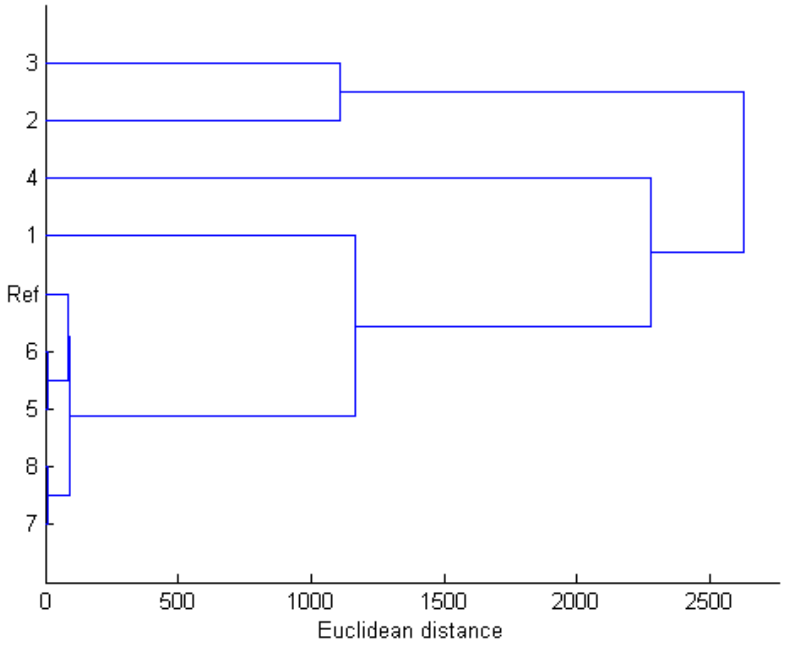

Figure 2. Dendrogram from the eight cases and the reference values from Tzanopoulou et al., 2006.

To the best of our knowledge, experimental data for 187Re NMR chemical shifts in solution are scarce. In fact, NMR results for Rhenium complexes are usually reported in the solid-state [46]. In view of this, the goal

of this work is to investigate the solvent and protein environment effects on σ values, we have used theoretical data for 187Re NMR shielding tensors (σ) obtained directly from GIAO-DFT calculations.

3.2. Enzymatic, solvent, and gas phase environments: Docking Studies and electronic structure calculations

Firstly, the position of the ReABT complex in the PI3K active site was analyzed by taking the overlap of the compound and the active ligand, N-{6-[2-(methylsulfanyl)pyrimidin-4-yl]-1, 3-benzothiazol-2-yl}acetamide (Figure 3). It is important to analyze this overlap to confirm that the active ligand and the ReABT have similar conformations in the enzyme active site, taking into account the overlap of functional groups and aromatic rings.

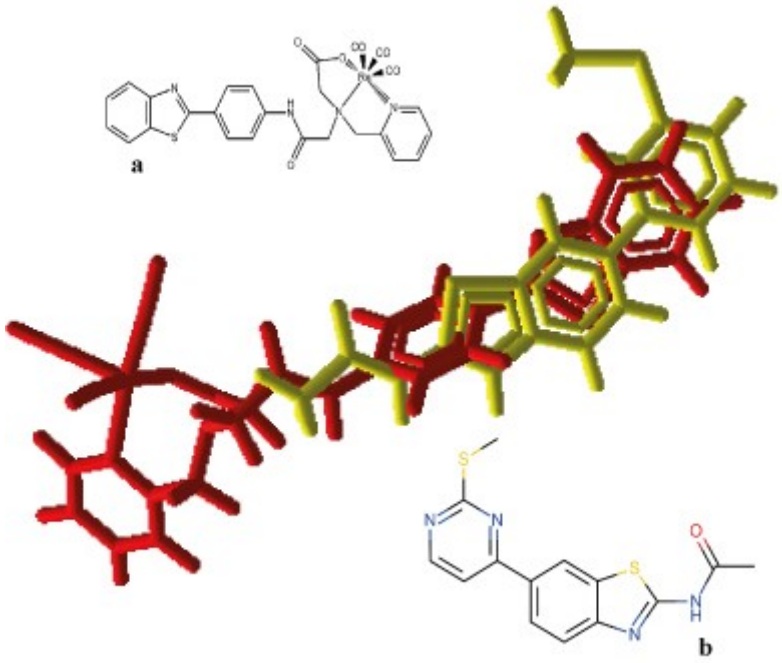

Figure 3. ReABT in red (structure in part a) and active ligand in yellow (structure in part b) docked in the PI3K (PDB code 3QJZ) active site.

The intermolecular interactions energy of the active ligand was equal to -121.17 kcal mol-1 and, for ReABT, -163.62 kcal mol-1. Our findings indicate that the complex ReABT could have good stability in the active site of the PI3K enzyme. Figure 4 shows the hydrogen bonds (H-Bonds) formed between ReABT and the amino acids residues Val882, Lys883, and Asp884.

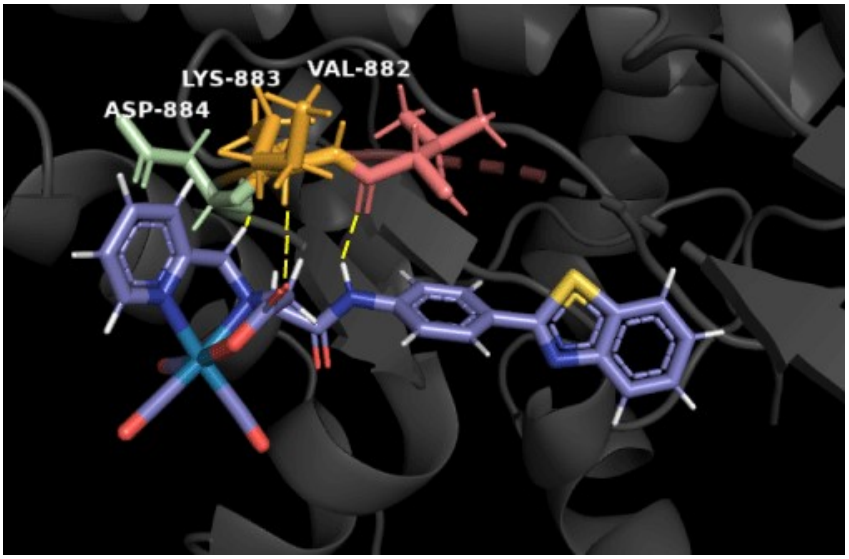

Figure 4. Complex ReABT with amino acids residues Asp884, Lys883, and Val 882. The H-Bonds are highlighted in yellow.

Now, the NMR calculation for the ReABT complex was also performed, considering the best protocol, using the CPCM solvation model, to evaluate the shielding tensors values for 187Re. Also, the same protocol was used to obtain σ(187Re) values in the active site of the PI3K enzyme. Thus, theoretical σ(187Re) values on different environments are reported in Table 4.

Table 4. Theoretical 187Re shielding tensors in different environments performed on PBE0/ZORA-TZVP and ZORA in the system Hamiltonian.

Environment	σ(^{187}Re) (ppm)
Gas phase	1630.49
Solution	1666.51
Protein (PI3K)	1514.65

These results point out that σ(187Re) values decrease around 150 ppm, ongoing from solvent to the protein environment. Our findings indicate that the complex Re(CO)3(NNO) conjugated with 2-(4'-aminophenyl) benzothiazole is a promising candidate for application as a spectroscopic probe, which could, in principle, help the breast cancer diagnosis.

4. CONCLUSIONS

A factorial model and a Hierarchical Cluster Analysis (HCA) were employed to determine the best calculation protocol for GIAO-DTF NMR calculations considering the ReABT complex. This analysis points out that the best functional is the PBE0, considering the relativistic effects, both in the (i) system Hamiltonian, including the ZORA implementation, and in the (ii) basis set, with SARC-ZORA-TZVP for Rhenium and ZORA-TZVP for all other atoms.

NMR calculations for ReABT point out that the $\sigma(^{187}Re)$ changes significantly when the complex is in the protein environment. Thus, from our theoretical findings, this complex is a promising spectroscopic probe and could be an alternative to the traditional contrast agents, such as Gd-based, once it presents activity in NMR spectroscopy and the metal center is less toxic.

SUPPLEMENTARY INFROMATION DESCRIPTION

Tables S1 and S2 are available in an additional document of Supplementary Materials and it shows the δ values for ^{1}H and ^{13}C; structure of ReABT with correspondent number elements.

CONFLICTS OF INTEREST

The authors declare that they have no conflicts of interest.

REFERENCES

1. Sung, H., et al., Global cancer statistics 2020: GLOBOCAN estimates of incidence and mortality worldwide for 36 cancers in 185 countries. CA: a cancer journal for clinicians, 2021. 71(3): p. 209-249. https://doi.org/10.3322/caac.21660

2. Siegel, R.L., K.D. Miller, and A. Jemal, Cancer statistics, 2019. CA: A Cancer Journal for Clinicians, 2019. 69(1): p. 7-34. https://doi.org/10.3322/caac.21551

3. Jafari, S.H., et al., Breast cancer diagnosis: Imaging techniques and biochemical markers. Journal of cellular physiology, 2018. 233(7): p. 5200-5213. https://doi.org/10.1002/jcp.26379

4. He, Z., et al., A review on methods for diagnosis of breast cancer cells and tissues. Cell Proliferation, 2020. 53(7): p. e12822. https://doi.org/10.1111/cpr.12822

5. Wang, L., Early Diagnosis of Breast Cancer. Sensors, 2017. 17(7). https://doi.org/10.3390/s17071572

6. Waks, A.G. and E.P. Winer, Breast cancer treatment: a review. Jama, 2019. 321(3): p. 288-300. doi:10.1001/jama.2018.19323

7. Galvão, E., et al., Breast cancer proteomics: a review for clinicians. Journal of cancer research and clinical oncology, 2011. 137(6): p. 915-925. https://doi.org/10.1007/s00432-011-0978-0

8. Barba, D., et al., Breast cancer, screening and diagnostic tools: All you need to know. Critical Reviews in Oncology/Hematology, 2021. 157: p. 103174. https://doi.org/10.1016/j.critrevonc.2020.103174

9. DeSantis, C.E., et al., Breast cancer statistics, 2019. CA: A Cancer Journal for Clinicians, 2019. 69(6): p. 438-451. https://doi.org/10.3322/caac.21583

10. Pereira, B.T.L., et al., Exploring EPR Parameters of ⁹⁹Tc Complexes for Designing New MRI Probes: Coordination Environment, Solvent, and Thermal Effects on the Spectroscopic Properties. Journal of Chemistry, 2017. 2017: p. 8102812. https://doi.org/10.1155/2017/8102812

11. Corrêa, S., et al., Hybrid Materials Based on Magnetic Iron Oxides with Benzothiazole Derivatives: A Plausible Potential Spectroscopy Probe. International Journal of Molecular Sciences, 2021. 22(8). https://doi.org/10.3390/ijms22083980

12. Gonçalves, M.A., et al., Probing thermal and solvent effects on hyperfine interactions and spin relaxation rate of δ-FeOOH(100) and [MnH3buea(OH)]2−: Toward new MRI probes. Computational and Theoretical Chemistry, 2015. 1069: p. 96-104. https://doi.org/10.1016/j.comptc.2015.07.006

13. Pereira, B.T.L., et al., First Attempts of the Use of 195Pt NMR of Phenylbenzothiazole Complexes as Spectroscopic Technique for the Cancer Diagnosis. Molecules, 2019. 24(21): p. 3970. https://doi.org/10.3390/molecules24213970

14. Tzanopoulou, S., et al., Synthesis, characterization, and biological evaluation of M (I)(CO) 3 (NNO) complexes (M= Re, 99mTc) conjugated to 2-(4-aminophenyl) benzothiazole as potential breast cancer radiopharmaceuticals. Journal of medicinal chemistry, 2006. 49(18): p. 5408-5410. https://doi.org/10.1021/jm0606387

15. Mancini, D.T., et al., 99Tc NMR as a promising technique for structural investigation of biomolecules: theoretical studies on the solvent and thermal effects of phenylbenzothiazole complex. Magnetic Resonance in Chemistry, 2014. 52(4): p. 129-137. https://doi.org/10.1002/mrc.4043

16. Tzanopoulou, S., et al., Evaluation of Re and 99mTc complexes of 2-(4′-aminophenyl) benzothiazole as potential breast cancer radiopharmaceuticals. Journal of medicinal chemistry, 2010. 53(12): p. 4633-4641. https://doi.org/10.1021/jm1001293

17. Machura, B., et al., Novel Re(I) tricarbonyl complexes of chelating ligands with aromatic N-heterocycle ring and aliphatic amine donor – Synthesis, spectroscopic characterization, X-ray structure and DFT calculations. Polyhedron, 2011. 30(13): p. 2275-2285. https://doi.org/10.1016/j.poly.2011.06.001

18. Machura, B., et al., Tricarbonyl rhenium(I) complex of benzothiazole – Synthesis, spectroscopic characterization, X-ray crystal structure and DFT calculations. Journal of Organometallic Chemistry, 2013. 724: p. 82-87. https://doi.org/10.1016/j.jorganchem.2012.10.020

19. Breitz, H.B., et al., Pharmacokinetics and normal organ dosimetry following intraperitoneal rhenium-186-labeled monoclonal antibody. Journal of Nuclear Medicine, 1995. 36(5): p. 754-761.

20. Mavroidi, B., et al., Palladium (II) and platinum (II) complexes of derivatives of 2-(4′-aminophenyl) benzothiazole as potential anticancer agents. Inorganica Chimica Acta, 2016. 444: p. 63-75. https://doi.org/10.1016/j.ica.2016.01.012

21. Long, N. and W.-T. Wong, The chemistry of molecular imaging. 2014: John Wiley & Sons.

22. Gonçalves, M.A., et al., Dynamics, NMR parameters and hyperfine coupling constants of the Fe3O4(100)–water interface: Implications for MRI probes. Chemical Physics Letters, 2014. 609: p. 88-92. https://doi.org/10.1016/j.cplett.2014.06.030

23. Srivastava, D. and S.N. Atluri, Computational nanotechnology: A current perspective. Computer Modeling in Engineering and Sciences, 2002. 3(5): p. 531-538.

24. Hassanzadeganroudsari, M., et al., Computational Chemistry to Repurposing Drugs for the Control of COVID-19. Biologics, 2021. 1(2): p. 111-128. https://doi.org/10.3390/biologics1020007

25. Ramalho, T.C. and M. Bühl, Probing NMR parameters, structure and dynamics of 5-nitroimidazole derivatives. Density functional study of prototypical radiosensitizers. Magnetic Resonance in Chemistry, 2005. 43(2): p. 139-146. https://doi.org/10.1002/mrc.1514

26. Bühl, M., et al., The DFT route to NMR chemical shifts. Journal of computational chemistry, 1999. 20(1): p. 91-105. https://doi.org/10.1002/(SICI)1096-987X(19990115)20:1<91::AID-JCC10>3.0.CO;2-C

27. Bühl, M., Density functional computation of 55Mn NMR parameters. Theoretical Chemistry Accounts, 2002. 107(6): p. 336-342. https://doi.org/10.1007/s00214-002-0338-x

28. Helgaker, T., M. Jaszunski, and K. Ruud, Ab initio methods for the calculation of NMR shielding and indirect spin-spin coupling constants. Chemical Reviews, 1999. 99: p. 293-352.

29. Pyykkö, P., Relativistic effects in chemistry: more common than you thought. Annual review of physical chemistry, 2012. 63: p. 45-64. https://doi.org/10.1146/annurev-physchem-032511-143755

30. Lin, Y.-S., et al., Long-Range Corrected Hybrid Density Functionals with Improved Dispersion Corrections. Journal of Chemical Theory and Computation, 2013. 9(1): p. 263-272. https://doi.org/10.1021/ct300715s

31. Pantazis, D.A., et al., All-electron scalar relativistic basis sets for third-row transition metal atoms. Journal of chemical theory and computation, 2008. 4(6): p. 908-919. https://doi.org/10.1021/ct800047t

32. van Wüllen, C., Molecular density functional calculations in the regular relativistic approximation: Method, application to coinage metal diatomics, hydrides, fluorides and chlorides, and comparison with first-order relativistic calculations. The Journal of chemical physics, 1998. 109(2): p. 392-399. https://doi.org/10.1063/1.476576

33. Nunes, C.A., et al., Chemoface: a novel free user-friendly interface for chemometrics. Journal of the Brazilian Chemical Society, 2012. 23: p. 2003-2010. https://doi.org/10.1590/S0103-50532012005000073

34. da Rocha, E.P., et al., Insights into the value of statistical models and relativistic effects for the investigation of halogenated derivatives of fluorescent probes. Theoretical Chemistry Accounts, 2016. 135(5): p. 135. https://doi.org/10.1007/s00214-016-1862-4

35. Ditchfield, R., Self-consistent perturbation theory of diamagnetism. Molecular Physics, 1974. 27(4): p. 789-807. https://doi.org/10.1080/00268977400100711

36. Wolinski, K., J.F. Hinton, and P. Pulay, Efficient implementation of the gauge-independent atomic orbital method for NMR chemical shift calculations. Journal of the American Chemical Society, 1990. 112(23): p. 8251-8260.

37. Zhao, Y. and D.G. Truhlar, A new local density functional for main-group thermochemistry, transition metal bonding, thermochemical kinetics, and noncovalent interactions. The Journal of chemical physics, 2006. 125(19): p. 194101. https://doi.org/10.1063/1.2370993

38. Adamo, C. and V. Barone, Toward reliable density functional methods without adjustable parameters: The PBE0 model. The Journal of chemical physics, 1999. 110(13): p. 6158-6170. https://doi.org/10.1063/1.478522

39. Autschbach, J., The calculation of NMR parameters in transition metal complexes. Principles and Applications of Density Functional Theory in Inorganic Chemistry I, 2004: p. 1-48. https://doi.org/10.1007/b97936

40. Zhao, Y. and D.G. Truhlar, Improved description of nuclear magnetic resonance chemical shielding constants using the M06-L meta-generalized-gradient-approximation density functional. The Journal of Physical Chemistry A, 2008. 112(30): p. 6794-6799. https://doi.org/10.1021/jp804583d

41. Jiménez-Pulido, S.B., et al., A combined experimental and DFT investigation on the structure and CO-releasing properties of mono and binuclear fac-Re I (CO) 3 complexes with 5-pyridin-2-ylmethylene-amino uracils. Dalton Transactions, 2016. 45(38): p. 15142-15154. DOI: 10.1039/C6DT02208A

42. Vícha, J., et al., Structure, solvent, and relativistic effects on the NMR chemical shifts in square-planar transition-metal complexes: assessment of DFT approaches. Physical Chemistry Chemical Physics, 2015. 17(38): p. 24944-24955. DOI: 10.1039/C5CP04214C

43. Neese, F., The ORCA program system. Wiley Interdisciplinary Reviews: Computational Molecular Science, 2012. 2(1): p. 73-78. DOI: 10.1002/WCMS.81

44. Thomsen, R. and M.H. Christensen, MolDock: a new technique for high-accuracy molecular docking. Journal of medicinal chemistry, 2006. 49(11): p. 3315-3321. https://doi.org/10.1021/jm051197e

45. D'Angelo, N.D., et al., Discovery and optimization of a series of benzothiazole phosphoinositide 3-kinase (PI3K)/mammalian target of rapamycin (mTOR) dual inhibitors. Journal of medicinal chemistry, 2011. 54(6): p. 1789-1811. https://doi.org/10.1021/jm1014605

46. Widdifield, C.M., F.A. Perras, and D.L. Bryce, Solid-state 185/187 Re NMR and GIPAW DFT study of perrhenates and Re 2 (CO) 10: chemical shift anisotropy, NMR crystallography, and a metal–metal bond. Physical Chemistry Chemical Physics, 2015. 17(15): p. 10118-10134. https://doi.org/10.1021/jm1014605

Supplementary Material

Insights into the value of statistical models, solvent and relativistic effects for investigating Re complexes of benzothiazole derivatives: potential spectroscopic probes

Gustavo A. Andolpho,[1] Elaine F. F. da Cunha,[1] and Teodorico C. Ramalho[1,2]

[1] Chemistry Department, Federal University of Lavras, P.O. Box 3037, 37200-900 Lavras, MG, Brazil.

[2] Center for Basic and Applied Research, Faculty of Informatics and Management, University of Hradec Kralove, Hradec Kralove, Czech Republic.

Correspondence should be addressed to Teodorico C. Ramalho; teo@ufla.br

Figure S1. Chemical structure of ReABT

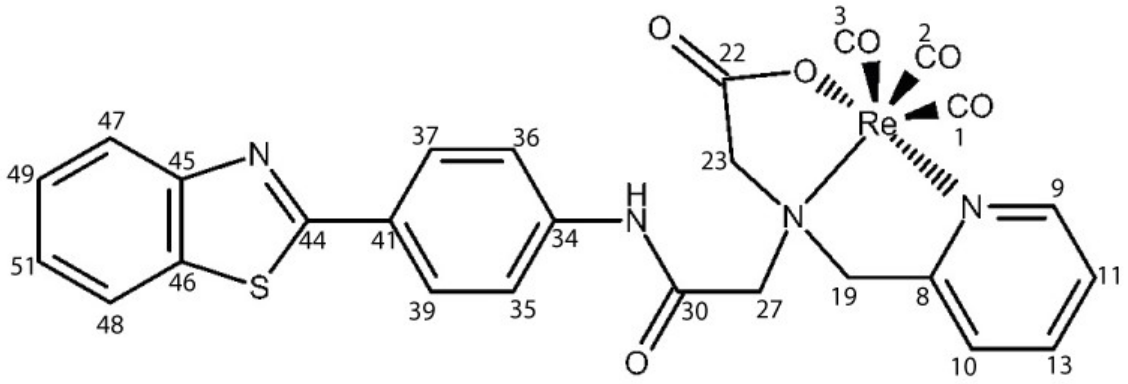

Table S1. Values, in ppm, for the eight cases used for ^{1}H chemical shifts calculations.

	δ(ppm) Cases							
#	1	2	3	4	5	6	7	8
9	8,154	-9,084	9,700	15,442	9,007	8,930	7,826	7,735
10	4,965	3,028	-2,859	-101,847	7,433	7,520	6,313	6,394
11	5,227	2,609	2,786	0,754	7,503	7,442	6,433	6,366
13	5,696	-2,711	-0,672	-95,040	7,937	7,941	6,946	6,944
19	-2,306	-13,407	-8,409	-3,480	4,076	4,222	3,250	3,375
19	4,417	15,779	-9,783	-65,988	3,529	3,449	2,938	2,846
23	6,907	-27,341	-14,681	4,207	2,426	2,416	1,727	1,690
23	10,314	2,452	-7,695	-72,746	4,982	5,075	4,167	4,239
27	3,207	-29,563	3,320	-72,713	3,147	3,297	2,419	2,555
27	7,995	7,342	-3,025	-4,664	3,187	3,393	2,560	2,742
NH	16,985	-16,445	14,505	15,579	7,716	7,816	6,751	6,837
35	8,096	3,986	5,714	17,993	7,201	7,238	5,885	5,921
36	10,744	12,954	12,884	1,274	9,174	9,227	5,915	7,965
37	8,328	5,480	6,210	18,685	9,055	9,074	7,680	7,701
39	7,277	9,692	7,624	1,248	8,123	8,149	6,884	6,911
47	7,998	7,532	6,293	11,455	8,319	8,331	7,117	7,131
48	7,891	8,169	6,583	6,405	8,044	8,054	6,962	6,963
49	7,492	7,269	6,059	7,155	7,685	7,690	6,609	6,617
51	7,426	7,439	6,082	6,662	7,560	7,559	6,497	6,498

Table S2. Values, in ppm, for the eight cases used for ^{13}C chemical shifts calculations.

	δ(ppm)							
	Cases							
#	1	2	3	4	5	6	7	8
1	-822,010	-576,100	-1028,013	60,035	154,056	158,739	179,459	182,989
2	-385,938	-75,935	-965,669	115,575	146,671	152,838	174,193	178,689
3	-184,803	-2725,580	-2730,726	60,809	151,383	156,173	176,909	180,585
8	121,962	106,745	12,495	-674,775	162,253	161,935	139,615	139,233
9	76,538	-14,881	32,182	-1456,921	158,116	156,344	140,869	139,172
10	138,538	82,947	110,707	-949,653	127,021	126,959	111,403	111,383
11	144,811	131,265	113,063	-38,223	129,195	129,228	112,352	112,365
13	123,479	62,469	115,418	-5,632	144,031	144,130	125,397	125,352
19	33,843	-286,735	-11,724	36,727	74,643	73,532	69,071	67,945
22	128,273	128,313	131,677	-623,700	176,771	176,567	161,280	161,056
23	63,295	-244,595	-22,676	76,893	64,486	65,157	57,463	58,144
27	47,089	-220,111	49,777	-865,183	68,604	68,812	61,130	61,398
30	161,654	85,428	138,254	-83,722	168,589	168,390	152,037	151,874
34	147,428	160,564	128,946	89,828	145,989	146,228	125,640	125,874
35	131,363	107,213	106,416	93,592	122,696	122,877	106,823	106,987
36	126,978	87,166	110,078	20,357	123,803	124,075	105,434	105,696
37	132,068	128,381	117,236	67,527	132,653	132,772	117,211	117,317
39	131,021	129,683	115,386	133,365	133,886	133,996	115,735	115,867
41	132,716	147,656	101,567	24,071	135,791	135,985	101,608	101,822
44	171,331	171,853	149,456	105,543	172,887	173,158	151,153	151,399
45	157,521	158,603	134,327	144,239	158,218	158,246	135,591	135,631
46	143,016	144,166	119,990	111,396	143,522	143,944	120,849	121,253
47	128,893	129,430	113,812	115,770	129,132	129,171	114,434	114,484
48	124,587	124,785	110,115	124,299	125,225	125,244	110,941	110,970
49	129,768	129,727	111,825	109,324	130,247	130,262	112,569	112,592
51	128,989	129,218	111,568	116,357	129,374	129,469	112,142	112,241